

DIPLOMA THESIS

**Optically preamplified
direct-detection
employing
time-domain filtering**

presented at the Technischen Universität Wien
Faculty of Electronics and Communication Engineering

by

Antonio Napoli
via Milano 21
I-13836 Cossato (BI) Italy

born on 5. September 1974 in Salerno
matriculation number 81424

Vienna, on 20 September 2002

Supervisors:

Univ. Prof. Dr. Walter R. Leeb
Dr. Martin M. Strasser

Abstract

In the last years optical amplifiers became commercially available. In the form of *erbium-doped fiber preamplifiers* they enable nearly quantum-limited receiver performance in the 1.5 μm wavelength range. Optically preamplified direct-detection became therefore an attractive receiver concept. Due to the high receiver sensitivity it is possible to reduce transmitter or mid-span amplifier requirements, to extend link distance and to provide additional margins. Performance optimization of optically preamplified receivers in the presence of optical noise (introduced by the optical amplifier's amplified spontaneous emission (ASE)) is today of major interest for the design of optical communication systems.

The aim of this work was to study merits and limitations of optical time-domain filtering in an optically preamplified direct-detection receiver. The time-domain filter is arranged between the receiver's optical filter and photodiode, and is implemented in the form of an electro-absorption modulator.

We then extended a tool for calculating the receiver sensitivity developed at the Technische Universitaet Wien by including the time-domain filter. Receiver noise was treated using the so-called advanced Gaussian model. Using this simulation tool we demonstrated that a time-domain filter can slightly improve the behavior of the optical receiver. Particularly, its influence became evident only when

- Energy signal suppression due to time-domain filtering is avoided. To this end the duty cycle of the time-domain filter function must exceed the duty cycle of the optical data signal,
- the electrical bandwidth of the electrical lowpass filter after the photodiode has a bandwidth less than twice the data rate of the signal,
- the extinction ratio of the time-domain filter function is larger than 12 dB,
- the misalignment between the optical data signal and the time-domain filter function is sufficiently small.

Under these conditions the receiver sensitivity, expressed in terms of photons per bit (ppb), is about 43 ppb. Compared to a receiver without time-domain filter this translates to an improvement of 0.6 dB.

The simulations were also compared to measurements performed in the optical laboratory. Measurements agreed well with simulations, confirming that

- the gain due to the time-domain filter may typically be as high as 0.6 dB,
- the electrical bandwidth may have distinct influence on the gain due to time-domain filtering,
- the optical bandwidth has negligible influence on the gain obtained by time-domain filtering.

Finally we report on an application of this work in the form of measurements of high-speed optical time division de-multiplexing systems.

Prefazione

Negli ultimi anni gli amplificatori ottici di tipo *erbium doped fiber preamplifier* sono divenuti commercialmente disponibili. Essi permettono il raggiungimento, in terza finestra, di prestazioni vicine al *quantum limit*. Per questo motivo i sistemi di trasmissione ottici in rivelazione diretta con preamplificatore ottico sono diventati una soluzione sistemistica attrattiva. Infatti, in seguito alla elevata *receiver sensitivity* è possibile ridurre gli accorgimenti al trasmettitore, aumentare la distanza massima di trasmissione ed ottenere margini aggiuntivi. L'ottimizzazione delle prestazioni di tali sistemi in presenza del rumore ottico (introdotto dall'amplificatore ottico e denominato *amplified spontaneous emission noise*) è oggi di fondamentale importanza all'interno dei sistemi di comunicazioni ottiche.

Il compito di questo lavoro di tesi è studiare i meriti e i limiti del filtraggio temporale in questo tipo di ricevitori ottici. Il filtro temporale è posizionato fra il filtro ottico al ricevitore ed il fotodiodo, ed è realizzato mediante un modulatore ottico ad elettroassorbimento.

Come primo passo è stato esteso un *tool*, sviluppato alla *Technische Universität Wien* per il calcolo della *receiver sensitivity*, al caso comprendente il filtraggio temporale. Il rumore al ricevitore è stato modellato mediante l'uso del così detto *advanced Gaussian model*. Usando il *tool* esteso abbiamo mostrato che un filtro temporale può leggermente migliorare il comportamento di un ricevitore ottico. In particolare, la sua influenza diventa importante solo quando

- è evitato il taglio di energia del segnale ottico da parte del filtro temporale. A questo fine il *duty cycle* del filtro temporale deve essere maggiore di quello del segnale ottico,
- la banda elettrica del filtro elettrico passabasso seguente al fotodiodo ha una banda minore del doppio del data rate,
- l'*extinction ratio* della funzione del filtro temporale è superiore a 12 dB,
- il *misalignment* fra il segnale ottico e la funzione di filtraggio temporale è trascurabile.

Sotto queste condizioni la *receiver sensitivity*, espressa in per bit, è circa 43 ppb, che comparato al caso di un ricevitore ottico senza filtro temporale comporta un guadagno di circa 0.6 dB.

Le simulazioni sono state successivamente anche comparate a misure effettuate in un laboratorio ottico. Le misure effettuate sono in buon accordo con le simulazioni e confermano che

- il guadagno del filtro temporale può essere tipicamente intorno a 0.6 dB,
- la banda elettrica può sensibilmente influenzare il guadagno fornito dal filtro temporale,

- la banda ottica ha un'influenza trascurabile sul guadagno fornito dal filtro temporale.

In fine riportiamo un'applicazione di questo lavoro relativo alle misure per sistemi ottici di tipo *optical time division multiplexing* ad elevata velocità.

Acknowledgement

I express my personal gratitude to Prof. Pierluigi Poggiolini for his constant help and interest, as well as for his continuous encouragement.

I thank Prof. Walter Leeb of the Technische Universität Wien for having constantly supervised me during my final project. His suggestions, comments and corrections have considerably improved the diploma work's quality.

I am very grateful to Dr. Martin Strasser for having been by me during these months. The continuous interaction and the numerous discussions with him allowed me to reach good results and to learn how to develop a scientific work. Dr. Martin Strasser, besides being a very excellent tutor, is for me a great friend.

A very special thank is for two women, who I strongly loved and who have strongly loved me, my mother Lucia and my girlfriend Anna. The First, as long as she enjoyed the life with us on this earth, gave me the power for pursuing my studies. The taking of my degree was a my mother's dream. The Second, driven by her infinite love and immense intelligence, helped me to overcome, in the best way, all the difficulties met by me.

The financial support of the *Hochschuljubiläumsstiftung der Stadt Wien* (grant number H-79/2001) made this work possible. I want to express my honest appreciation for funding the electroabsorption modulators used extensively in this work.

Last but not the least, I express my very special thanks to my family and to my girlfriend's family for having always encouraged me and supported at any time during my universities studies.

Ringraziamenti

Esprimo la mia gratitudine al Prof. Pierluigi Poggiolini per il suo costante aiuto ed interessamento, nonché per il suo continuo incoraggiamento.

Ringrazio il Prof. Walter Leeb della Technische Universität Wien per avermi costantemente seguito durante questo mio lavoro. I suoi suggerimenti, commenti e le sue correzioni hanno notevolmente migliorato la qualità della lavoro di tesi.

Sono enormemente grato al Dr. Martin Strasser per essermi stato sempre vicino in questi mesi. La continua interazione e le numerose discussioni avute con lui mi hanno consentito di raggiungere buoni risultati e di apprendere come sviluppare una ricerca scientifica. Dr. Martin Strasser, oltre ad essere un validissimo collaboratore, è per me un grande amico.

Un grazie del tutto speciale va alle due Donne che più ho amato e che più mi hanno amato, mia madre Lucia e, la mia fidanzata Anna. La Prima, finchè è rimasta qui con noi su questa terra, mi ha dato sempre la forza per andare avanti. Il conseguimento della laurea era un suo sogno. La Seconda con il suo infinito amore e la sua straordinaria intelligenza mi ha aiutato a superare nel migliore dei modi tutte le difficoltà incontrate.

Il supporto finanziario del *Hochschuljubiläumsstiftung der Stadt Wien* (contratto numero H-79/2001) ha reso possibile la realizzazione di questo lavoro. Voglio esprimere la mia sincera gratitudine per aver potuto utilizzare, grazie al citato aiuto finanziario, il modulatore ottico ad elettroassorbimento ampiamente adoperato in questa tesi.

Ultimi, ma non per questo meno importanti, ringrazio la mia famiglia ed la famiglia della mia fidanzata, per avermi sempre incoraggiato e sostenuto, nel corso di questi anni di Università.

Contents

1	Introduction	1
1.1	Optically preamplified direct detection (DD) receiver	2
1.2	Sensitivity and quantum limit	2
1.3	Concepts of time-domain filtering	3
1.4	Intention of this diploma work	4
2	Detection noise analysis	7
2.1	Noise formulae for time-domain filtering	7
2.2	Quantum limit of preamplified DD receiver	10
2.3	Bit error probability	14
2.4	Spectral effect of time-domain filtering	14
3	Modelling	19
3.1	Transmitter	19
3.1.1	Modulation format	19
3.2	Receiver	21
3.2.1	Optical preamplifier	21
3.2.2	Spectral filter	22
3.2.3	Time-domain filter	23
3.2.4	Photodiode and detection electronics	28
3.3	Limitations of SimTool	28
4	Simulation results	32
4.1	Introduction of time-domain filtering	32
4.2	Influence of duty cycle and pulse shape on receiver sensitivity	34
4.3	Influence of the electrical bandwidth	38
4.4	Influence of extinction ratio on receiver sensitivity	43
4.5	Influence of misalignment on receiver sensitivity	44
5	Measurements	48
5.1	Measurement setup	48
5.1.1	Transmitter	48
5.1.2	Receiver	51
5.1.3	Signal monitoring	52
5.2	Measurements	53

5.2.0.1	Basic influence of time-domain filter	53
5.2.0.2	Measurements at different electrical bandwidths	53
5.2.0.3	Measurements at different optical bandwidth	54
5.3	Comparison of measurements and simulation	54
5.3.1	Sensitivity dependence on electrical bandwidth	55
5.3.2	Sensitivity dependence on optical bandwidth	55
5.3.3	Conclusions	56
6	Summary	58
6.1	Summary of the work presented	58
6.2	Application: OTDM measurements	59
	Bibliography	62

Chapter 1

Introduction

The ever emerging customer services of Internet, mobile communication and telephony increases the bandwidth demand of data networks continuously. Optical communication system are able to transmit the huge amount of information and the networks are requested to improve steadily their quality and speed of transmission.

Figure 1.1 shows the basic optical communication system consisting of (i) a data transmitter, usually a laser generating optical data pulses, (ii) a channel, being a optical fiber for terrestrial data networks or free-space channel for space applications, and (iii) a receiver, where the main device is a photodiode converting optical power in an electrical signal. This diploma work deals with a special type of optical receivers namely *optically preamplified direct-detection (DD) receiver*.

In the last years optical amplifier (i.e erbium doped fiber amplifier) became commercially available and optical exemplification enables nearly quantum limit receiver performance in the $1.5 \mu m$ range. Optically preamplified direct-detection became therefore an attractive receiver concept. Due to the high receiver sensitivity it is possible to reduce transmitter or mid-span amplifiers requirements, to extend link distance and to provide additional margins [1]. Performance optimization of optically preamplified receivers in the presence of optical noise is today of major interest for the design of optical communication systems.

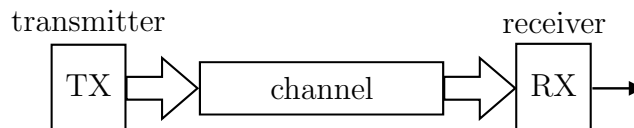


Figure 1.1: Basic concept of communication system

1.1 Optically preamplified direct detection (DD) receiver

Figure 1.2 shows a typical optically preamplified direct-detection receiver [2]. An optical data signal $e_{in}(t)$, is received and amplified by an optical preamplifier (i.e erbium doped fiber amplifier (EDFA)), providing a high gain of typically 30 to 40 dB. The EDFA introduces *amplified spontaneous emission noise* (ASE noise) being the dominant noise source at the receiver ¹. The power spectral density of ASE noise is given by $N_{ASE} = hfFG/2$ [3], where hf is the photon energy at the light frequency f , h denotes the Plank's constant, G is the gain of the optical amplifier and F (*always* ≥ 2 [3]) its noise figure.

To suppress ASE noise, the optical preamplifier is followed by an optical bandpass filter. The photodiode performs the optoelectronic conversion of the optical signal, corrupted by white gaussian ASE noise into an electrical current. The detected current is filtered by an electrical lowpass filter to further suppress noise. Finally, the electrical signal is sampled at the time instants $t = t_s + kT$, where $k \in \mathbb{N}$ and T is the inverse of data rate R . A decision gate extracts the digital data by comparing the noisy signal to a threshold.

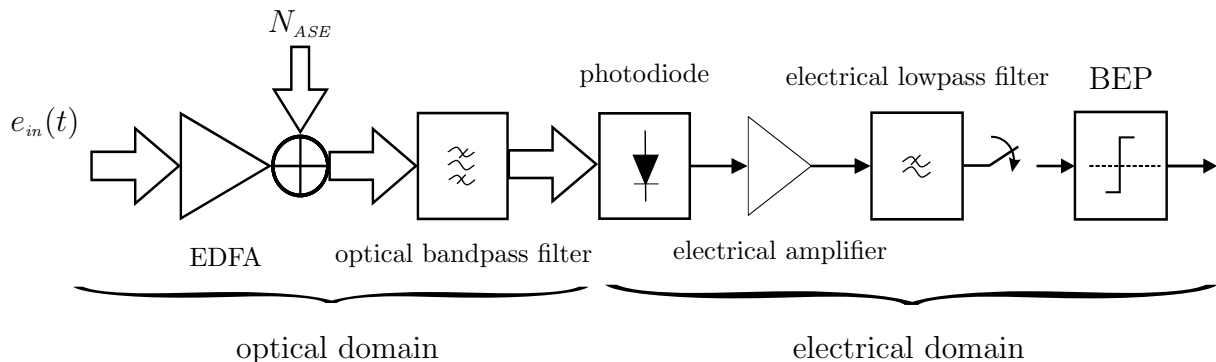


Figure 1.2: Optically preamplified direct-detection receiver

1.2 Sensitivity and quantum limit

The main parameter which characterizes the performance of an optical receiver is called *sensitivity* n_s . It is defined as the *received number of photons per bit (ppb) to achieve a bit error probability (BEP) of 10^{-9}* . The absolute minimum level of the sensitivity is called *quantum limit* n_q [4]. In the context of this work the sensitivity is expressed in terms of sensitivity penalty γ_q relative to quantum limit

¹Figure 1.4 (b) shows the power data signal corrupted by ASE noise as function of the optical wavelength

$$\gamma_q = 10 \log_{10} \left(\frac{n_s}{n_q} \right) [dB]. \quad (1.1)$$

If all noise sources, except shot noise, are negligible, a direct detection (DD) receiver achieves its quantum limit of $n_q = 10 \text{ ppb}$ [4]. When optical preamplification is employed the best achievable sensitivity is $n_s = 20 \text{ ppb}$ [5]. In contrast coherent receivers have different quantum limits. An ideal heterodyne receiver requires $n_q = 18 \text{ ppb}$ for detection at $BEP = 10^{-9}$, whereas $n_q = 9 \text{ ppb}$ is for homodyne receiver [4], both in case of phase shift keying.

The mentioned quantum limit of 20 ppb for optically preamplified DD receiver can only be achieved when the optimum modulation format (differential phase shift keying (DPSK)) is applied. In this work the modulation format OOK (on-off keying) is considered only. For that special case the quantum limit is $n_q = 41 \text{ ppb}$. That value is found by using Gaussian noise statistics [6]. However the actual probability density function of detection noise is not exactly Gaussian [7]. Hence the exact quantum limit of optically preamplified DD receiver employing on-off keying modulation (OOK) is 38 ppb [6, 8].

1.3 Concepts of time-domain filtering

This section gives the reader a rough idea of how *time-domain filter* (TF) works and what are the main effects on the optical data signal. Note, the term time-domain filtering is not a standard denomination in optical communication engineering, but it is only used by the author of this work.

Figure 1.3 shows an optical preamplified direct-detection (DD) receiver which is *extended* by a time-domain filter. The TF is placed between the optical filter and the photodiode. Basically the TF filter performs a *multiplication in time* of the spectrally filtered optical signal with a time-domain filter function $f_{TF}(t)$. This time filter function $f_{TF}(t)$ is applied to the TF. The filter function is periodic with T ($T = 1/R$), and it satisfies the relation $f_{TF}(t) = f_{TF}(t + T)$. Further, the filter function is assumed to be exactly synchronized with optical data signal $e_f(t)$. Generally, the shape of $f_{TF}(t)$ is arbitrary, but in the context of this work it is assumed to be always rectangular or cosine-squared.

As mentioned, above the time-domain filter performs a multiplication of the optical filtered signal with the filter function. Mathematically, this can be expressed as

$$e_{TF}(t) = e_f(t) \cdot f_{TF}(t), \quad (1.2)$$

where $e_{TF}(t)$ is the time-filtered signal after the time-domain filter.

Figure 1.4 shows a comparison between optical filtering and time-domain filtering, where the left (right) column represents spectral (time-domain) filtering.

- **Spectral filtering**

Figure 1.4 (a) depicts the power spectrum of the received data signal $e_{in}(t)$ corrupted by ASE noise. Figure 1.4 (b) shows the magnitude of the optical filter

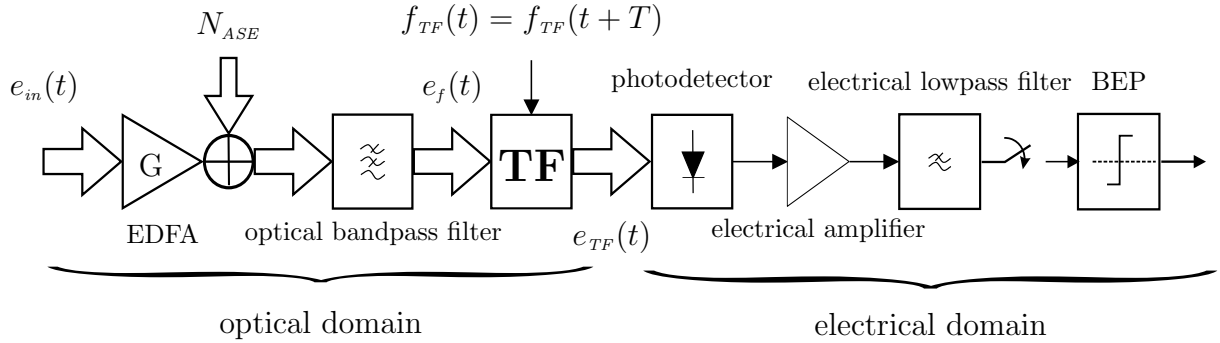


Figure 1.3: Optically preamplified direct-detection (DD) receiver employing time-domain filtering

transmission function $|H_o(\lambda)|$. The optical filter reduces ASE noise, since the noise bandwidth is about 60 nm [9] and the optical filter bandwidth is typically smaller than 1 nm. The signal bandwidth is assumed to be smaller than the optical filter bandwidth B_o , hence the optical filter does not distort the data signal. Figure 1.4 (c) shows the filtered optical signal.

- **Time-domain filtering**

Figure 1.4 (d) represents the spectrally filtered data signal in time. Here so-called *return-to-zero* (RZ) signals are employed [10], characterized by a parameter called *RZ factor*, defined as [11]

$$D = \frac{T}{\tau} \tag{1.3}$$

where T represents the *bit duration* and τ is the *pulse duration*. The parameter D is the inverse duty-cycle, e.g an RZ factor of $D = 5$ is equal to a duty cycle of 20 %. Figure 1.4 (e) shows the time-domain filter function. The assumed shape is rectangular. The inverse duty cycle of the time-domain filter function is called D_{TF} , being defined in the same way as it was done for the data signal.

The effect of time-domain filtering is explained by Fig. 1.4 (e), where *noise between two bits is suppressed due to the multiplication of the data signal and the filter function*. When the TF function is transparent, signal and noise are passed through the time-domain filter; otherwise only noise, as the data signal is supposed to be perfectly synchronized with TF, is suppressed. Figure 1.4 (f) displays the product of $e_f(t)$ and $f_{TF}(t)$, being the time-domain filtered signal.

1.4 Intention of this diploma work

The goal of this work is to clarify the effect of time-domain filtering in preamplified DD receivers (i.e. its impact on receiver sensitivity).

Appendix 2 gives the theoretical basis of this work. The first part presents advanced Gaussian noise statistics [10] providing the variances $\sigma^2(t)$ for ASE-ASE noise and ASE-signal noise. Further, the influence of TF on the ASE spectrum is analyzed. *Appendix 3* describes the simulation tool **SimTool** being developed at the Institute for Communication and Radio Frequency Engineering (Vienna University of Technology) for analyzing optical preamplified direct detect receivers. The limits of the simulation tool are discussed. Then this simulator is extended by time-domain filter functions. *Appendix 4* shows simulation results for receiver sensitivity obtained by using **SimTool** employing TF. The influence of pulse shape, duty-cycle, electrical and optical bandwidth, extinction ratio and degrading effects on receiver sensitivity is discussed. *Appendix 5* presents experimental results obtained in the laboratory. The experimental results are compared to the simulations. Good agreement is demonstrated. The last *Appendix 6* discussed one application of TF, e.g. the emulation of *electrical time division multiplexed* receivers (ETDM) by *optical time division multiplexed* receivers (OTDM) [12].

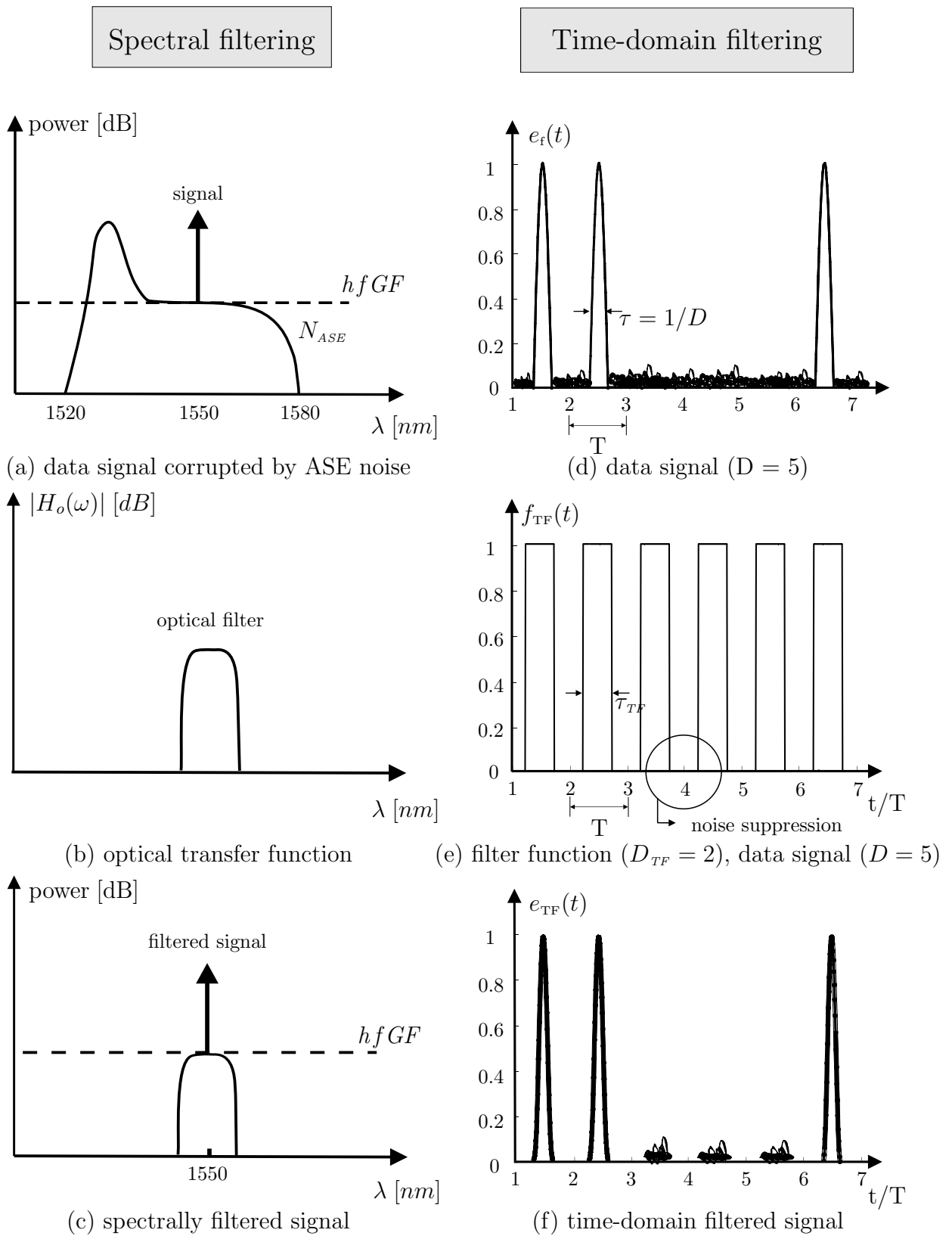


Figure 1.4: Comparison of spectral filtering with time-domain filtering

Chapter 2

Detection noise analysis

Appendix 1 presented the basic set-up for an optically preamplified direct-detection receiver. Appendix 2 analyzes and models the detection noise of an optical preamplified DD receiver employing time-domain filtering. Firstly, the variance of detection noise is calculated and the resulting sensitivity is derived. Secondly, the influence of TF on the power spectrum of ASE noise is discussed.

2.1 Noise formulae for time-domain filtering

This section is based on the noise analysis given in [8] and further extensions performed by M.M. Strasser and P.J. Winzer. Figure 2.2 shows the block diagram of an optically preamplified DD receiver employing TF. The following noise analysis is based on this receiver structure.

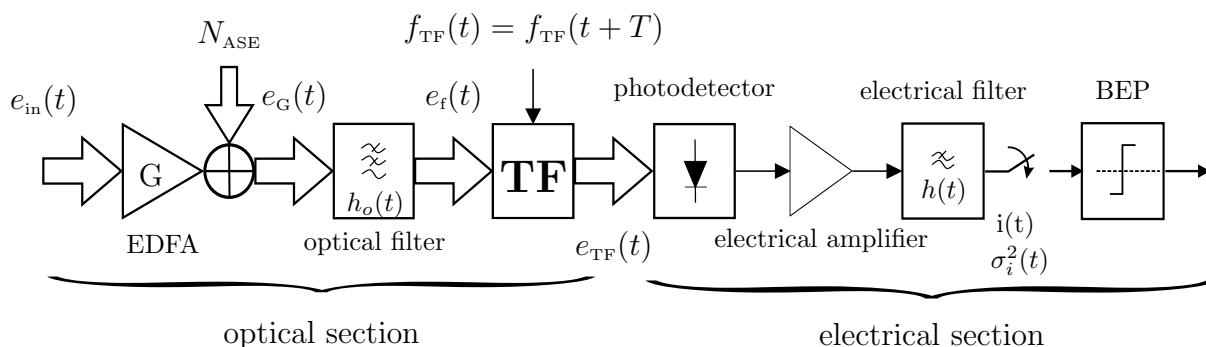


Figure 2.1: Optically preamplified direct-detection receiver employing time-domain filtering.

An arbitrary, complex, optical field $\mathbf{e}_{\text{in}}(t)$ is received and preamplified by a low-noise high-gain optical amplifier (EDFA), with gain G and noise figure F . Due to the optical preamplification the incoming signal is additionally disrupted by amplified spontaneous emission (ASE), modelled as stochastic Gaussian process $\mathbf{n}_{\text{ASE}}(t)$. Hence the preampli-

fied optical field becomes also a stochastic process

$$\mathbf{e}_G(t) = Ge_{in}(t) + \mathbf{n}_{ASE}(t), \quad (2.1)$$

which is assumed to be stationary, circularly symmetric and complex [8, 13].

The signal and the noise are spectrally filtered by an optical filter, characterized by the time transfer function $h_o(t)$, in order to reduce ASE noise. The filtered optical field reads as

$$\mathbf{e}_f(t) = [G_o e_{in}(t) + \mathbf{n}_{ASE}(t)] * h_o(t), \quad (2.2)$$

where the symbol '*' denotes the mathematical operator for temporal convolution, which is expressed by

$$x(t) * y(t) = \int_{-\infty}^{+\infty} x(\tau)y(t - \tau)dt. \quad (2.3)$$

To further suppress noise, the optical field is temporally filtered by multiplication with a T -periodic function $f_{TF}(t) = f_{TF}(t + T)$, which satisfies $f_{TF}(t) \geq 0$ and $\Im\{f_{TF}(t)\} = 0$. The operator $\Im\{\cdot\}$ stands for the imaginary part. The time-domain filtered field results in a cycle-stationary process $\mathbf{e}_{TF}(t) = \mathbf{e}_f(t) \cdot f_{TF}(t)$ with period T .

According to [13], the ensemble average of the detected signal is

$$\langle i(t) \rangle = S \langle |\mathbf{e}_{TF}(t)|^2 \rangle * h(t), \quad (2.4)$$

where $h(t)$ denotes the entire transfer function of the photo detector, electrical amplifier, and lowpass filter; S is the overall optoelectronic conversion factor of the detection chain. The operator $\langle \cdot \rangle$ stands for

$$\langle x \rangle = \int_{-\infty}^{+\infty} \xi p_x(\xi) d\xi \quad (2.5)$$

and calculates the expectancy of the stochastic process \mathbf{x} , where $p_x(\xi)$ is the probability density function of the stochastic process \mathbf{x} [14]. By assuming that the average optical power at the detector is

$$P(t) = \langle |\mathbf{e}_{TF}(t)|^2 \rangle \quad (2.6)$$

and $\langle \mathbf{n}_{ASE}(t) \rangle = 0$, the ensemble average showed in Eq. 2.4 can be simplified under the constraint of stationary noise to

$$\langle i(t) \rangle = S[P(t) * h(t)] + SP_n[f_{TF}(t)^2 * h(t)], \quad (2.7)$$

where $P_n = \langle |\mathbf{n}(t)|^2 \rangle$ denotes the average noise power [13].

The variance of the detected stochastic process is given by [13]

$$\sigma_{\mathbf{i}} = Se \langle |\mathbf{e}_{\text{TF}}(t)|^2 \rangle * h(t)^2 + S^2 \iint_{-\infty}^{+\infty} C_{|\mathbf{e}_{\text{TF}}(t)|^2}(\tau, \tilde{\tau}) h(t - \tau) h(t - \tilde{\tau}) d\tau d\tilde{\tau}, \quad (2.8)$$

where $C_{|\mathbf{e}_{\text{TF}}(t)|^2} = \langle |\mathbf{e}_{\text{TF}}(\tau)|^2 |\mathbf{e}_{\text{TF}}(\tilde{\tau})|^2 \rangle - \langle |\mathbf{e}_{\text{TF}}(\tau)|^2 \rangle \langle |\mathbf{e}_{\text{TF}}(\tilde{\tau})|^2 \rangle$ is the autocovariance function of $|\mathbf{e}_{\text{TF}}(t)|^2$ and e denotes the elementary charge. The first term of the right hand of Eq. 2.8 stands for the variance of signal-shot noise

$$\sigma_{\mathbf{i}, \text{s-shot}} = Ce p(t) * h(t)^2 \quad (2.9)$$

and ASE-shot noise

$$\sigma_{\mathbf{i}, \text{ASE-shot}} = Ce P_n f_{\text{TF}}(t) * h(t)^2 \quad (2.10)$$

which can be neglected under the assumption of high gain preamplification [15]. The second term of Eq. 2.8 expands to

$$\begin{aligned} & C^2 \iint_{-\infty}^{+\infty} \left(\underbrace{\langle |\mathbf{e}_f(\tau) f_{\text{TF}}(\tau)|^2 |\mathbf{e}_f(\tilde{\tau}) f_{\text{TF}}(\tilde{\tau})|^2 \rangle}_{\mathbb{A}} - \right. \\ & \left. - \underbrace{\langle |\mathbf{e}_f(\tau) f_{\text{TF}}(\tau)|^2 \rangle \langle |\mathbf{e}_f(\tilde{\tau}) f_{\text{TF}}(\tilde{\tau})|^2 \rangle}_{\mathbb{B}} \right) h(t - \tau) h(t - \tilde{\tau}) d\tau d\tilde{\tau}. \end{aligned} \quad (2.11)$$

By applying the Gaussian momentum theorem [13]

$$\langle \mathbf{x}_1 \mathbf{x}_2 \dots \mathbf{x}_N \rangle = \begin{cases} 0 & , N = \text{odd} \\ \sum_{\text{all pairs}} \langle \mathbf{x}_1 \mathbf{x}_2 \rangle \langle \mathbf{x}_3 \mathbf{x}_4 \rangle \dots \langle \mathbf{x}_{N-1} \mathbf{x}_N \rangle & , N = \text{even} \end{cases}, \quad (2.12)$$

for the random variables \mathbf{x}_n , $n = 1 \dots N$, we obtain $\langle \mathbf{n}(\tau) \mathbf{n}(\tilde{\tau}) \rangle = 0$, $\langle \mathbf{n}(\tau) \mathbf{n}(\tilde{\tau}) \mathbf{n}^*(\tilde{\tau}) \rangle = 0$ and

$$\langle |\mathbf{n}(\tau)|^2 |\mathbf{n}(\tilde{\tau})|^2 \rangle = \langle |\mathbf{n}(\tau)|^2 \rangle \langle |\mathbf{n}(\tilde{\tau})|^2 \rangle + \langle \mathbf{n}^*(\tau) \mathbf{n}(\tilde{\tau}) \rangle \langle \mathbf{n}(\tau) \mathbf{n}^*(\tilde{\tau}) \rangle \quad (2.13)$$

since the realizations of the stochastic process $\mathbf{n}(t)$ at different time instants yield statistically independent random variables $\mathbf{n}(\tau)$. By applying these results, the terms \mathbb{A} and \mathbb{B} in Eq. 2.11 simplify to

$$\begin{aligned} \mathbb{A} = & p(\tau) p(\tilde{\tau}) + 2\Re\{e_f(\tau) e_f^*(\tilde{\tau}) |f_{\text{TF}}(\tau)|^2 |f_{\text{TF}}(\tilde{\tau})|^2 \langle \mathbf{n}^*(\tau) \mathbf{n}(\tilde{\tau}) \rangle\} + \\ & + p(\tau) \langle |\mathbf{n}(\tilde{\tau}) f_{\text{TF}}(\tilde{\tau})|^2 \rangle + p(\tilde{\tau}) \langle |\mathbf{n}(\tau) f_{\text{TF}}(\tau)|^2 \rangle + \langle |\mathbf{n}(\tau) f_{\text{TF}}(\tau)|^2 |\mathbf{n}(\tilde{\tau}) f_{\text{TF}}(\tilde{\tau})|^2 \rangle \end{aligned} \quad (2.14)$$

$$\begin{aligned} \mathbb{B} = & p(\tau) p(\tilde{\tau}) + p(\tau) \langle |\mathbf{n}(\tilde{\tau}) f_{\text{TF}}(\tilde{\tau})|^2 \rangle + p(\tilde{\tau}) \langle |\mathbf{n}(\tau) f_{\text{TF}}(\tau)|^2 \rangle + \\ & + \langle |f_{\text{TF}}(\tau)|^2 |\mathbf{n}(\tau)|^2 \rangle \langle |f_{\text{TF}}(\tilde{\tau})|^2 |\mathbf{n}(\tilde{\tau})|^2 \rangle \end{aligned} \quad (2.15)$$

and the difference results in

$$\begin{aligned} \mathbb{A} - \mathbb{B} = & 2\Re\{e_f(\tau)e_f^*(\tilde{\tau})|f_{\text{TF}}(\tau)|^2|f_{\text{TF}}(\tilde{\tau})|^2\langle\mathbf{n}^*(\tau)\mathbf{n}(\tilde{\tau})\rangle\} + \\ & + |f_{\text{TF}}(\tau)|^2|f_{\text{TF}}(\tilde{\tau})|^2|\langle\mathbf{n}^*(\tau)\mathbf{n}(\tilde{\tau})\rangle|^2. \end{aligned} \quad (2.16)$$

Inserting Eq. 2.16 in 2.11 yields the variance of signal-ASE beat noise

$$\sigma_{\mathbf{i},\text{s-ASE}} = 2C^2 \iint_{-\infty}^{+\infty} |f_{\text{TF}}(\tau)|^2|f_{\text{TF}}(\tilde{\tau})|^2\Re\{e_f(\tau)e_f^*(\tilde{\tau})\langle\mathbf{n}^*(\tau)\mathbf{n}(\tilde{\tau})\rangle\}h(t-\tau)h(t-\tilde{\tau})d\tau d\tilde{\tau} \quad (2.17)$$

and the variance of ASE-ASE beat noise

$$\sigma_{\mathbf{i},\text{ASE-ASE}} = C^2 \iint_{-\infty}^{+\infty} |f_{\text{TF}}(\tau)|^2|f_{\text{TF}}(\tilde{\tau})|^2|\langle\mathbf{n}^*(\tau)\mathbf{n}(\tilde{\tau})\rangle|^2h(t-\tau)h(t-\tilde{\tau})d\tau d\tilde{\tau}. \quad (2.18)$$

2.2 Quantum limit of preamplified DD receiver

This section calculates the quantum limit - being the maximum receiver sensitivity given in photons per bit - of optically preamplified DD receivers using the advanced Gaussian noise model. The quantum limit n_q found is used in the further context of this work as reference value. A system employing time-domain filtering has the same quantum limit of a system without.

The subsequently calculated quantum limit is the sensitivity of an idealized system where the only noise source is ASE noise introduced by the EDFA.

Signal and noise are handled separately and the bit error BEP is [?]

$$BEP = \frac{1}{2} \left[Q\left(\frac{|i_0 - I_{th}|}{\sigma_0}\right) + Q\left(\frac{|i_1 - I_{th}|}{\sigma_1}\right) \right], \quad (2.19)$$

where i_0 and i_1 are the sampled current for the '0'-bits and the '1'-bits, respectively; σ_0 and σ_1 are the standard deviations of the sampled detection noise, I_{th} is the threshold, and $Q(x)$ is defined as

$$Q(x) = \frac{1}{\sqrt{2\pi}} \int_x^{\infty} e^{-\frac{y^2}{2}} dy. \quad (2.20)$$

The quantum limit is achieved by using a *matched optical filter* [14], which is defined as

$$h_o(t) = e_G^*(-t). \quad (2.21)$$

The matched filter maximizes the SNR (Signal-to-Noise Ratio) and thus minimizes the BEP for a given received signal. The transfer function of the detection block is

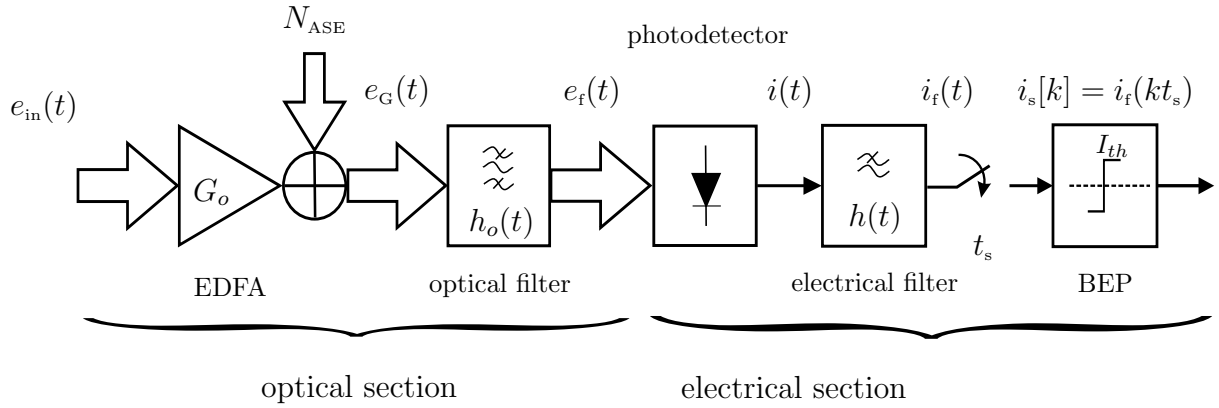


Figure 2.2: Optically preamplified direct-detection receiver

$h(t) = \delta(t)$, hence $i_f(t) = i(t)$. The resulting variance of the ASE-ASE beat noise before the sampler is [10]

$$\begin{aligned}
 \sigma_{ASE-ASE}^2 &= S^2 N_{ASE}^2 \iint_{-\infty}^{\infty} |r_{h_o}(\tau - \tilde{\tau})|^2 h(t - \tau) h(t - \tilde{\tau}) d\tau d\tilde{\tau} \\
 &= S^2 N_{ASE}^2 \iint_{-\infty}^{\infty} |r_{h_o}(\tau - \tilde{\tau})|^2 \delta(t - \tau) \delta(t - \tilde{\tau}) d\tau d\tilde{\tau} \\
 &= S^2 N_{ASE}^2 |r_{h_o}(0)|^2
 \end{aligned} \tag{2.22}$$

where the function $r_{h_o}(t)$ is the optical filter's autocorrelation function

$$r_{h_o}(t) = \int_{-\infty}^{\infty} h_o(\tau) h_o(t - \tau) d\tau \tag{2.23}$$

For the signal-ASE beat noise the variance becomes

$$\begin{aligned}
 \sigma_{s-ASE}^2(t) &= 2S^2 N_{ASE} \Re \left\{ \iint_{-\infty}^{\infty} e_i(t - \xi) e_f^*(t - \eta) r_{h_o}(\eta - \xi) h(\eta) h(\xi) d\eta d\xi \right\} \\
 &= 2S^2 N_{ASE} \Re \left\{ \iint_{-\infty}^{\infty} e_i(t - \xi) e_f^*(t - \eta) r_{h_o}(\eta - \xi) \delta(\eta) \delta(\xi) d\eta d\xi \right\} \\
 &= 2S^2 N_{ASE} |p(t)|^2 r_{h_o}(0)
 \end{aligned} \tag{2.24}$$

where the power of the filtered signal reads as

$$|p(t)|^2 = \int_{-\infty}^{\infty} e_f(t)e_f^*(t)dt. \quad (2.25)$$

In the case of a matched filter the optimum sampling instance is $t_s = 0$, hence

$$i(0) = S |e_f(0)|^2 \quad (2.26)$$

$$\sigma_{ASE-ASE}^2(0) = S^2 N_{ASE}^2 |r_{h_o}(0)|^2 \quad (2.27)$$

$$\sigma_{s-ASE}^2(0) = 2S^2 N_{ASE} |p(t)|^2 r_{h_o}(0) \quad (2.28)$$

By inserting $i_0 = 0$, $i_1 = i(0)$, $\sigma_0^2 = \sigma_{ASE-ASE}^2$, $\sigma_1^2 = \sigma_{s-ASE}^2 + \sigma_{ASE-ASE}^2$, the BEP becomes

$$BEP = \frac{1}{2} \left[Q \left(\frac{|i_0 - I_{th}|}{\sigma_0} \right) + Q \left(\frac{|i_1 - I_{th}|}{\sigma_1} \right) \right] \quad (2.29)$$

$$= \frac{1}{2} \left[Q \left(\frac{I_{th}}{SN_{ASE}|r_{h_o}(0)|} \right) + Q \left(\frac{S|e_f(0)|^2 - I_{th}}{\sqrt{2S^2 N_{ASE} |p(t)|^2 r_{h_o}(0) + S^2 N_{ASE}^2 |r_{h_o}(0)|^2}} \right) \right] \quad (2.30)$$

Denoting $\frac{I_{th}}{SN_{ASE}|r_{h_o}(0)|} = \rho$ leads to

$$BEP = \frac{1}{2} \left[Q(\rho) + Q \left(\frac{\frac{|e_f(0)|^2}{N_{ASE} r_{h_o}(0)} - \rho}{\sqrt{\frac{2|e_f(0)|^2}{N_{ASE} r_{h_o}(0)} + 1}} \right) \right]. \quad (2.31)$$

For a matched filter the correlation function is

$$r_{h_o}(0) = \int_{-\infty}^{\infty} |h_o(\tau)|^2 d\tau = \int_{-\infty}^{\infty} |e_G(\tau)|^2 d\tau = e_f(0) \quad (2.32)$$

and the mean received signal energy of a single bit is

$$\bar{E} = \frac{1}{2} \cdot \int_{-\infty}^{\infty} |e_G(\tau)|^2 d\tau = \frac{e_f(0)}{2}. \quad (2.33)$$

This can also be expressed as

$$\bar{E} = hf\bar{n}G_o, \quad (2.34)$$

where hf is the photon energy and \bar{n} represents the average number of photons per bit. The power spectral density of the noise is [3]

$$N_{ASE} = n_{sp}hf(G_o - 1) = n_{sp}hf(G_o - 1) \approx hfG_o = \frac{\bar{E}}{\bar{n}}. \quad (2.35)$$

We assume an ideal optical amplifier with $n_{sp} = 1$ and $G \gg 1$. Therefore the BEP formula given in Eq. 2.31 simplifies to

$$BEP = \frac{1}{2} \left[Q(\rho) + Q\left(\frac{2\bar{n} - \rho}{\sqrt{4\bar{n} + 1}}\right) \right]. \quad (2.36)$$

Subsequently the optimum threshold ρ is obtained by minimizing the BEP

$$\begin{aligned} \frac{\partial BEP}{\partial \rho} &= 0 \\ e^{-\frac{1}{2}\rho^2} - \frac{1}{\sqrt{4\bar{n} + 1}} e^{-\frac{1}{2}\left[\frac{2\bar{n} - \rho}{\sqrt{4\bar{n} + 1}}\right]^2} &= 0 \\ -\frac{1}{2} \ln(4\bar{n} + 1) - \frac{1}{2} \left[\frac{2\bar{n} - \rho}{\sqrt{4\bar{n} + 1}} \right]^2 &= -\frac{1}{2}\rho^2 \\ -(4\bar{n} + 1) \ln(4\bar{n} + 1) - 4\bar{n}^2 + 4\bar{n}\rho - \rho^2 &= -4\bar{n}\rho^2 - \rho^2 \\ \rho^2 + \rho - \bar{n} - \frac{(4\bar{n} + 1)}{4\bar{n}} \ln(4\bar{n} + 1) &= 0 \end{aligned} \quad (2.37)$$

yielding the optimum threshold

$$\rho_1 = -\frac{1}{2} + \sqrt{\frac{1}{4} + \bar{n} + \frac{(4\bar{n} + 1)}{4\bar{n}} \ln(4\bar{n} + 1)}. \quad (2.38)$$

By solving

$$BEP = \frac{1}{2} \left[Q(\rho_1) + Q\left(\frac{2\bar{n} - \rho_1}{\sqrt{4\bar{n} + 1}}\right) \right] \doteq 10^{-9} \quad (2.39)$$

the mean number of photons per bit necessary to reach a BEP of 10^{-9} is obtained. A numerical solution of Eq. 2.39 yields $n_{TF} = 41.0$ ppb, hence the so-called quantum limit is

$$\boxed{\bar{n}_q = 41\text{ppb}}$$

Note, for the calculations of the quantum limit Gaussian noise statistics were used. In real systems, the probability density function of detection noise is not exactly Gaussian, hence the exact quantum limit is 38 ppb [8]. However, in the context of this work the Gaussian approximation is used.

2.3 Bit error probability

The method to calculate the bit error probability (BEP) in `SimTool`, which is a software tool for simulating optically preamplified DD receivers, is discussed in this section.

After the electrical lowpass filter, the electrical current $i_f(t)$, corrupted by colored ASE noise, is detected. An ideal switch clocked at $R = 1/T$ samples the signal at the time instants $t = t_s + kT$ with $k \in \mathbb{N}$. A decision gate extracts the digital data by comparing the noisy signal $i(t)$ with the threshold I_{th} . The BEP at sample instant t_s and with decision threshold I_{th} is calculated according to [11]

$$BEP(t_s, i_{th}) = \frac{1}{2^m - 1} \left\{ \sum_{k_0} \frac{1}{2} \operatorname{erfc} \left[\frac{i_{th} - i_0(t_s + k_0T)}{\sqrt{2}\sigma(t_s + k_0T)} \right] + \sum_{k_1} \frac{1}{2} \operatorname{erfc} \left[\frac{i_1(t_s + k_1T) - i_{th}}{\sqrt{2}\sigma(t_s + k_1T)} \right] \right\}, \quad (2.40)$$

where the indices k_0 and k_1 are used to distinguish between the $2^{m-1} - 1$ transmitted "0"-bits and $2^{m-1} - 1$ "1"-bits of the pseudo random sequence (PN) sequence. Here the complementary error function is defined by

$$\operatorname{erfc}(x) = \frac{2}{\sqrt{\pi}} \int_x^{\infty} e^{-t^2} dt. \quad (2.41)$$

Clearly, Gaussian noise statistics have been assumed. It has been proved [6, 16, 17] that Gaussian approximation yields accurate results in the case of *on-off keying* modulation (OOK) and DD receivers. The minimum BEP is obtained by a two dimensional minimization, expresses as

$$\{i_{th}, t_s\}_{opt} = \min_{i_{th}, t_s} \{BEP\}. \quad (2.42)$$

This yields the optimum decision threshold and sampling instant. These values depend on the signal shape, the variance of detection noise, and the average power of the optical input field $e_{in}(t)$. Usually the optimum threshold is close to "0"-bit current, since as a result of the signal-dependent noise, the noise variance of the sampled "1"-bit is significantly larger than the noise variance of the sampled "0"-bit.

2.4 Spectral effect of time-domain filtering

Below the effect of time-domain filtering on the spectrum of ASE noise is analyzed. The system considered is shown in Fig. 2.3.

To simplify the following calculations, the spectral transfer function of the optical filter is assumed to be rectangular, i.e.

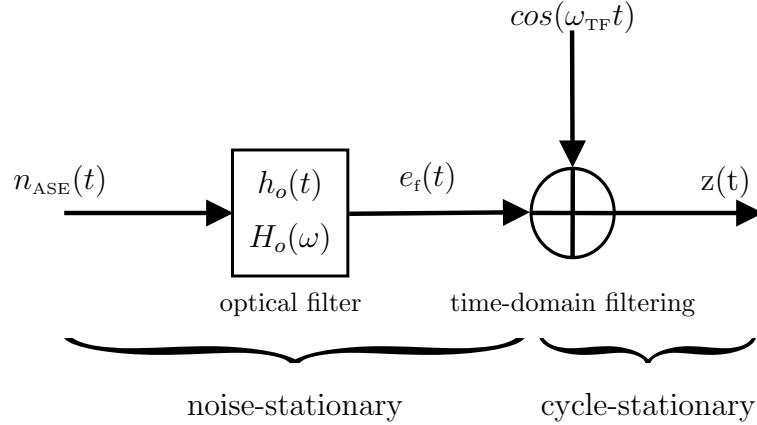


Figure 2.3: System model for the analysis of the effect of TF on ASE noise spectrum

$$H_o(\omega) = \begin{cases} 1 & \text{if } |\omega| < \omega_c, \\ 0 & \text{else} \end{cases}, \quad (2.43)$$

where $2\omega_c$ indicates the optical filter bandwidth. To simplify the description of this phenomena we denote the rectangular function of optical filter, shown in Fig. 2.4, $rect(\omega/\omega_c)$. The expression in the time domain is given by performing the Fourier transformation of $rect(\omega/\omega_c)$, yielding

$$h_o(t) = \frac{\sin(\omega_{TF}t)}{\pi t}. \quad (2.44)$$

The spectrally filtered ASE noise reads as

$$y(t) = n_{ASE}(t) * h_o(t). \quad (2.45)$$

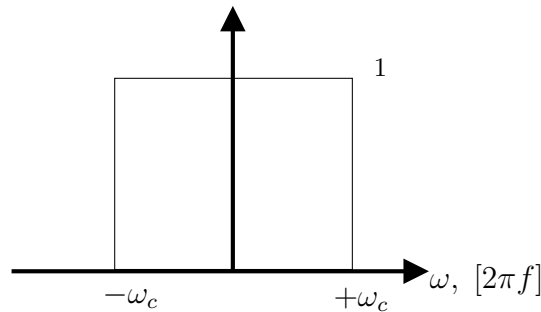


Figure 2.4: *rectangular function*

The process described by Eq. 2.45 is a Gaussian stationary process. By performing the Fourier transform on this expression it is possible to study the effect of TF on the spectrum of ASE noise. Since the signal to analyze is not deterministic, we calculate the equivalent *power spectral density function* $G_x(\omega)$ and *autocorrelation function* $R_x(\tau)$,

instead of the Fourier transform. The relation between $G_x(\omega)$ and $R_x(\tau)$ is

$$G_x(\omega) = \mathcal{F}\{R_x(\tau)\} \quad (2.46)$$

where the symbol $\mathcal{F}\{\cdot\}$ is the Fourier transform operator.

By applying this operator to Eq. 2.45, the power spectral density function of the ASE noise can be written as

$$G_y(\omega) = G_n(\omega)|H_o(\omega)|^2 = N_{\text{ASE}}|H_o(\omega)|^2. \quad (2.47)$$

The autocorrelation function of this process is

$$\mathcal{F}\{G_y(\omega)\} = R_y(\tau) = N_{\text{ASE}} \frac{\sin(\omega_{\text{TF}} t)}{\pi t}. \quad (2.48)$$

The spectrally filtered signal $y(t)$ is time-domain filtered by multiplication with the periodic filter function $f_{\text{TF}}(t) = f_{\text{TF}}(t + T)$ resulting in

$$z(t) = y(t) f_{\text{TF}}(t + T). \quad (2.49)$$

In order to keep the complexity of the calculations low the time-domain filter function is assumed to be

$$f_{\text{TF}}(t) = \cos^2(\omega_{\text{TF}} t). \quad (2.50)$$

The autocorrelation function of the signal $z(t)$ reads as

$$R_z(\tau, t + \tau) = \langle z(t)z(t + \tau) \rangle, \quad (2.51)$$

yielding

$$R_z(\tau, t + \tau) = \langle \{y(t) \cos^2(\omega_{\text{TF}} t) y(t + \tau) \cos^2[\omega_{\text{TF}} (\tau + t)]\} \rangle. \quad (2.52)$$

The filter function is deterministic, therefore the autocorrelation function becomes

$$R_z(\tau, t + \tau) = \cos^2(\omega_{\text{TF}} t) \cos^2[\omega_{\text{TF}} (\tau + t)] R_y(\tau). \quad (2.53)$$

The last expression tells us that the process is not stationary anymore, but cycle-stationary. Since is not possible to calculate the power spectral density function (PSDF) of a cycle-stationary process, the cycle-stationary process $z(t)$ is transformed into a quasi-stationary process $\tilde{z}(t)$ by applying [14]

$$R_{\tilde{z}(\tau)} = \frac{1}{T_{\text{B}}} \int_0^{T_{\text{B}}} R_z(t, t + \tau) dt. \quad (2.54)$$

When inserting Eq. 2.53 in Eq. 2.54 we obtain

$$R_{\tilde{z}(\tau)} = \frac{1}{T_{\text{B}}} R_y(\tau) \int_0^{T_{\text{B}}} \cos^2(\omega_{\text{TF}} t) \cos^2(\omega_{\text{TF}} t + \tau) dt, \quad (2.55)$$

yielding the autocorrelation function of the quasi-stationary process $\tilde{z}(t)$

$$R_{\tilde{z}}(\tau) = R_y(\tau) \left[\frac{1}{4} + \frac{1}{8} \cos(2\omega_{\text{TF}}\tau) \right]. \quad (2.56)$$

The corresponding PSDF, given by the convolution between $R_y(\tau)$ and the expression within the brackets, reads as

$$G_{\tilde{z}}(\omega) = \frac{1}{4} N_{\text{ASE}} \left\{ \text{rect} \left(\frac{\omega}{2\omega_0} \right) + \frac{1}{4} \text{rect} \left[\frac{\omega}{2(\omega_0 + 2\omega_{\text{TF}})} \right] + \frac{1}{4} \text{rect} \left[\frac{\omega}{2(\omega_0 - 2\omega_{\text{TF}})} \right] \right\}. \quad (2.57)$$

The PSDF according to Eq. 2.57 is showed in Fig. 2.5 under the assumption of $\omega_o = 5\omega_{\text{TF}}$, in order to visualize the influence of time-domain filtering.

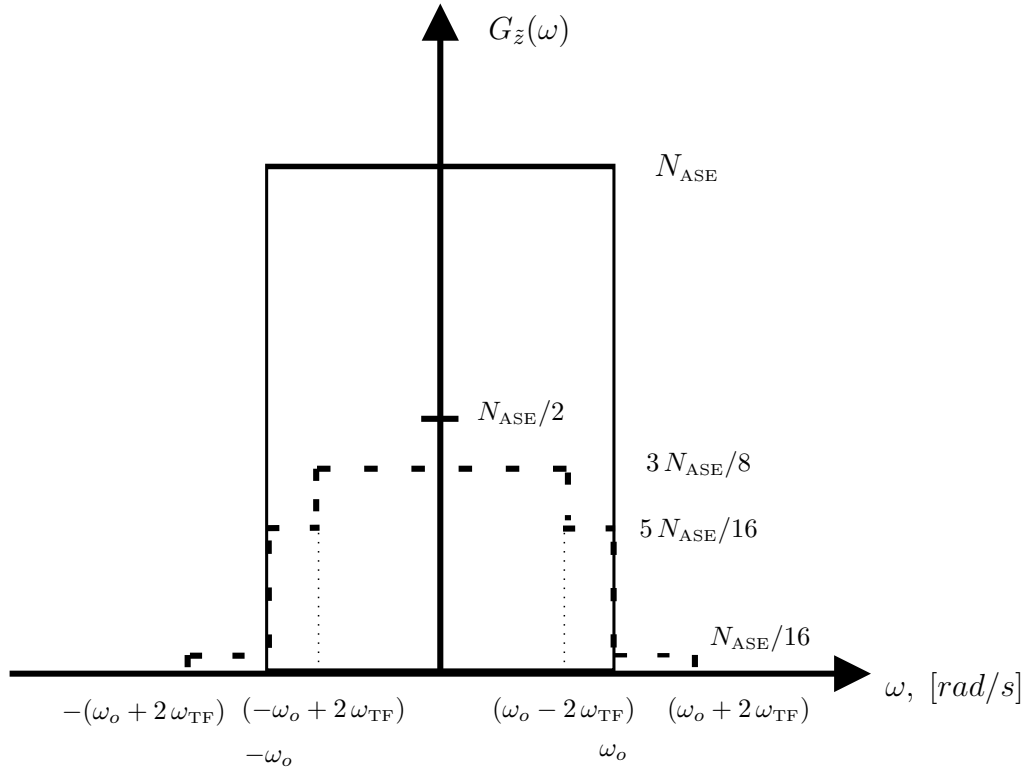


Figure 2.5: The solid line represents the spectrum of spectrally filtered ASE noise and dashed represents time-domain filtered ASE noise

The PSDF consists of three $\text{rect}(\cdot)$ terms: the first is centered at $\omega = 0$, given by the convolution between $G_y(\omega)$ and a dirac functional $\delta(\omega)$, the second and the third terms are spectrally shifted due to the TF modulation. The spectrally filtered ASE noise

is modulated and spectrally widened and attenuated due to TF. Figure 2.5 shows the effect of TF on the ASE noise spectrum. The solid line represents the ASE noise before filtering by TF (i.e after optical filter), the dashed line is the ASE noise time-domain filtered. Time-domain filtering typically reduces ASE by more than 50 %.

Chapter 3

Modelling

This appendix models an optical back-to-back communication system. The system uses on-off keying (OOK) modulation and the receiver is an optically preamplified direct-detection receiver employing time-domain filtering. Firstly, a detailed transmitter and receiver model is presented, which is implemented in the system simulator `SimTool`. Secondly, the simulation limits of `SimTool` are pointed out and finally, simulation results are presented.

3.1 Transmitter

The transmitter generates an on-off keying (OOK) pseudo-noise (PN) bit sequence. The PN sequence [14] contains $2^m - 1$ bits where m is the sequence order. On-off keying is a digital modulation format sending optical pulses representing the "1"-bits as shown in Fig. 3.1. For "0"-bits no signal power is transmitted. The modulation format OOK can be divided in two formats: *Non-Return-to-Zero* (NRZ) coding and *Return-to-Zero* (RZ) coding.

3.1.1 Modulation format

For the back-to-back case the *receiver input* is given by the transmitted signal. We denote its equivalent baseband representation $e_{\text{in}}(t)$. The input field is normalized to let its squared magnitude yield the optical input power $p(t) = |e_{\text{in}}(t)|^2$. The optical power waveform representing a single "1"-bit $p_1(t)$ is specified within the time interval $[0, (1+\alpha)\tau_p]$ as

$$p_1(t) = \begin{cases} \frac{E_1}{2\tau_p} \left\{ 1 - \sin \left[\frac{\pi}{\alpha\tau_p} \left(|t - (1+\alpha)\frac{\tau_p}{2}| - \frac{\tau_p}{2} \right) \right] \right\} & , \quad t \in \{[0, \alpha\tau_p] \vee [\tau_p, (1+\alpha)\tau_p]\} \\ \frac{E_1}{\tau_p} & , \quad t \in [\alpha\tau_p, \tau_p] \end{cases} \quad (3.1)$$

where E_1 is the *optical energy* for a "1"-bit. It is defined as

$$E_1 = \int_{-\infty}^{+\infty} p_1(t) dt, \quad (3.2)$$

where τ_p denotes the *effective pulse duration* being defined as [11]

$$\tau_p = \frac{\int_{-\infty}^{+\infty} p_1 dt}{\max_t \{p_1(t)\}} = \frac{E_1}{\max_t \{p_1(t)\}}. \quad (3.3)$$

The parameter α , which can vary between $[0,1]$, is called *roll-off factor*. It is connected with rise and fall time of the data pulses and specifies the pulse shape. Varying α from 0 to 1, the pulse shape changes from ideal rectangular pulse (see Fig. 3.1 (a)) to $\cos^2(t)$ -like (see Fig. 3.1 (b)). Logical "0"-bits are ideally represented by absence the of an optical signal.

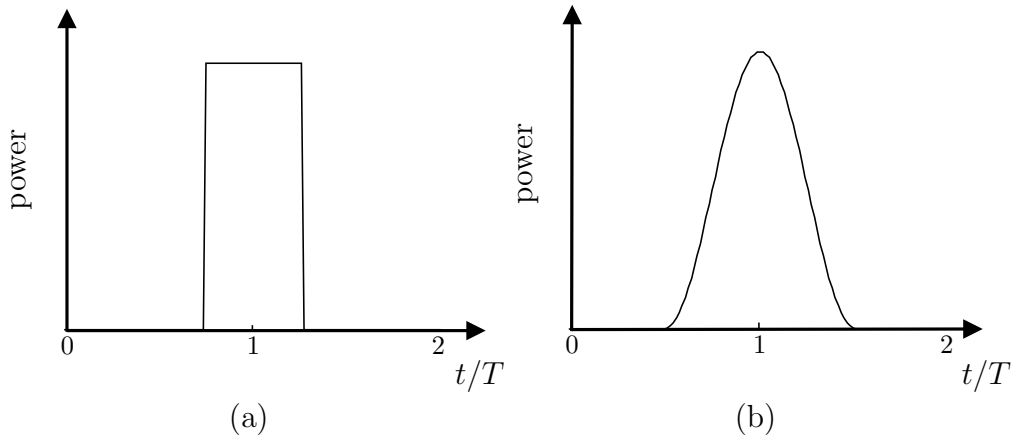


Figure 3.1: Plot (a) shows a "1"-bit of rectangular pulse shape, obtained by setting the parameter $\alpha = 0$; Plot (b) shows the case of a $\cos^2(t)$ -like pulse $\alpha = 1$.

By using the bit duration T and τ_p , the D factor is defined as

$$D = \frac{T}{\tau_p}, \quad (3.4)$$

which is equal to the inverse of the duty cycle. Setting $\tau_p = T$ yields an isolated NRZ "1"-bit pulse, having a duty cycle of 100% ($D = 1$). Figure 3.2 (a) shows a sequence of NRZ pulses. When $\tau_p = d \cdot T$ ($|d| < 1$), an RZ pulse with duty cycle $d = 1/D$ is generated. The D factor for RZ pulses is always larger than 1. Figure 3.2 (b) displays the same bit sequence for RZ coding as shown for the case of NRZ.

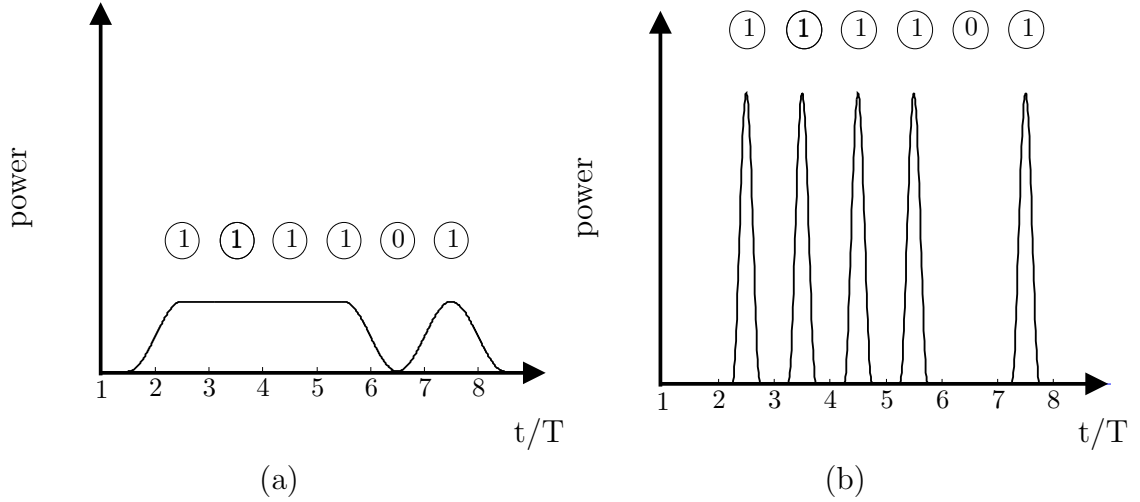


Figure 3.2: Modulation format: Plot (a) represents a non-return-to-zero (NRZ) coded data signal with $D = 1$; Plot (b) shows a return-to-zero (RZ) coded signal with $D = 4$. Both data signals consist of $\cos^2(t)$ -like pulses (i.e. $\alpha = 1$).

3.2 Receiver

3.2.1 Optical preamplifier

The optical amplifier is the first device of the considered receiver shown in Fig. 2.2. As mentioned in Sec. 1.3 and shown in Fig. 1.4 (a), an EDFA amplifies with a high gain of usually 30...40 dB and it introduces ASE noise. ASE noise is characterized by Eq. 2.35. In this equation, n_{sp} can be expressed as [18]

$$n_{sp} = \frac{F}{2(1 - \frac{1}{G})}. \quad (3.5)$$

where F denotes the EDFA's noise figure. The high gain of the EDFA is essential since it makes the beat noise between ASE and signal and ASE with itself the dominating noise sources at the receiver. It is also important to keep the noise figure F low in order to reduce the ASE noise. The minimum noise figure is $F = 3 \text{ dB}$ [9].

As ASE noise is not polarized, a polarization filter can be used to suppress ASE noise power in the state of polarization being orthogonal to the signal's state of polarization. The result is a reduction of ASE noise power by 3dB. However, polarization filtering does not necessarily increase the sensitivity of the receiver in a significant way, since the most dominating noise term is beat noise between signal and ASE, which only incorporates one state of polarization of ASE. Also, a polarization filter introduces insertion losses. This does not worsen the optical signal-noise-ratio (OSNR) but decreases the effective gain of the preamplifier which in turn is essential for highly sensitive reception.

3.2.2 Spectral filter

An optical bandpass filter is used to reduce the ASE noise in the frequency domain. The optical bandpass filter is described by its dimensionless baseband field transfer function $B(f)$. We distinguish between two optical filters, namely: a Fabry Pèrot filter (FPF) and a fiber Bragg gratings (FBG).

- **Fabry Pèrot Filter**

The transfer function of a FPF can be approximated by the Lorentzian function [19, 20], which is valid for the practically relevant case of high etalon finesse, i.e. narrow bandwidth. The filter transfer function is

$$B_{\text{FPF}}(f) = \frac{1}{1 + 2jf/B_o} \quad (3.6)$$

where B_o denotes the filter's 3dB bandwidth. The corresponding complex baseband impulse response $b(t)$ is the inverse Fourier transform of $B(f)$.

- **Fiber Bragg Grating**

The FBG uses a circulator to convert the FBG's bandstop characteristic into a bandpass characteristic, resulting in [20, 21]

$$B_{\text{FBG}}(f) = \frac{1}{\tan(\kappa l)} \frac{-j\kappa \sin[\beta(f)l]}{j\beta(f) \cos[\beta(f)l] - (2\pi f/v_g) \sin(\beta(f)l)} \quad (3.7)$$

where $\beta(f)$ stands for

$$\beta(f) = \sqrt{(2\pi f/v_g)^2 - \kappa^2} \quad (3.8)$$

and κ is the grating coupling coefficient, kept constant at a typical value of 6 cm^{-1} [21]; l and v_g are the grating length and the group velocity, respectively. The values were appropriately set to achieve the desired 3dB bandwidth at a constant sidelobe suppression ratio (SLSR) of 7dB. The 3dB bandwidth B_o is defined as

$$|B_{\text{FBG}}(0)| = \sqrt{2} \cdot |B_{\text{FBG}}(B_o/2)|. \quad (3.9)$$

Figures 3.3 (a) and (b) show the power transmissions $|B(f)|^2$ as function of the frequency for both filters types. The power transmissions are normalized to unity; any insertion loss (IL) of the optical filters can readily be accounted for by using a reduced effective optical amplifier gain of $G(1 - IL)$.

In the case of the FPF, the transition of the passband to the rejection band is more smooth. Hence at the same 3dB bandwidth B_o , the FBG suppresses noise more efficiently than a FPF.

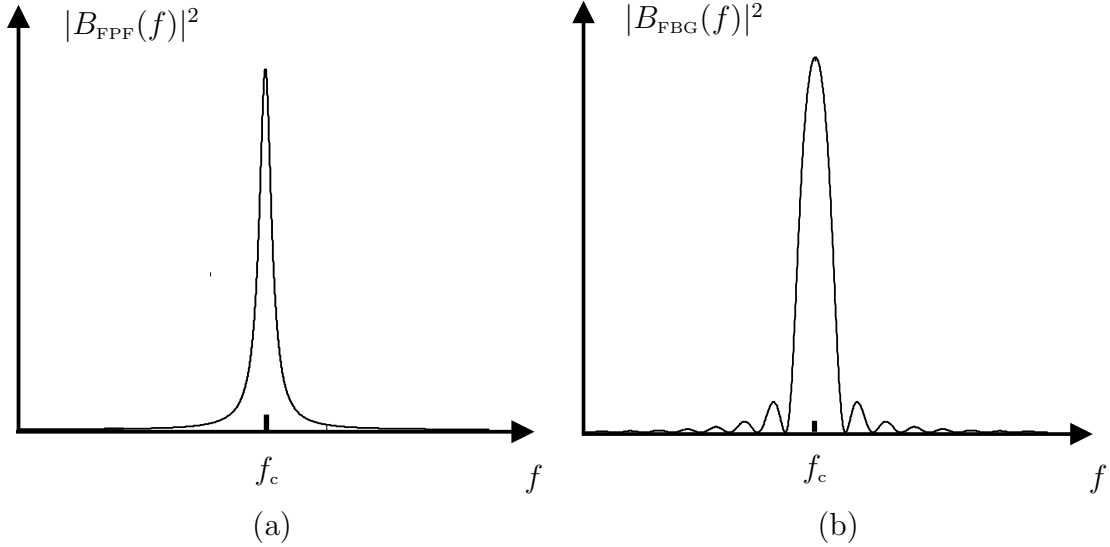


Figure 3.3: Optical filters: Power transmission of a Fabry Pèrot filter (a) and a fiber Bragg Gratings filter (b) as a function of the frequency $f - f_c$; f_c denotes the filter's center frequency.

3.2.3 Time-domain filter

An electroabsorption modulator (EAM) can not only be used for intensity modulation but also as time-domain filter. In the first case it modulates the light produced by a laser to generate optical data pulses. In the second case, a time-domain filter function is applied to the EAM in order to further suppress noise at the optical receiver.

Since electroabsorption (EA) in semiconductor multiquantum well (MQW) structures is approximately 50 times larger than in bulk semiconductors [22], most commercially available EAMs are based on MQW structures. MQW EAM's exploit the so-called quantum-confined Stark effect (QCSE). The band gap energy of a MQW is made slightly larger than the photon energy of the transmitted light, thus the modulator is transparent and has negligible absorption. When an electric field is applied perpendicularly to the MQW structure, the band energy slightly reduces and laser light is absorbed. The stronger the electric field is, the larger the absorption is [22]. The optical power transmitted by an EAM can be quantitatively expressed as function of the reverse bias voltage (V) in the form [23]

$$p(V) = p_0 e^{-\left(\frac{V}{V_0}\right)^a}, \quad (3.10)$$

where p_0 is the output power at maximum transmission ($V = 0$) of the EAM and V_0 is the voltage where the transmitted power $p(V)$ has dropped to $1/e$ of p_0 . The voltage V_0 depends on the modulator type and is usually $V_0 < 1 V$ [23, 24, 25]. The technological parameter a can range between 3...4 for MQW EAM's [23]. Figure 3.4 (a) shows the influence of this technological parameter on the transmitted power as function of the reverse bias voltage. A large a means a steeper decrease of the transmission characteristic, hence MQW modulators with larger parameter a require a smaller reverse modulation

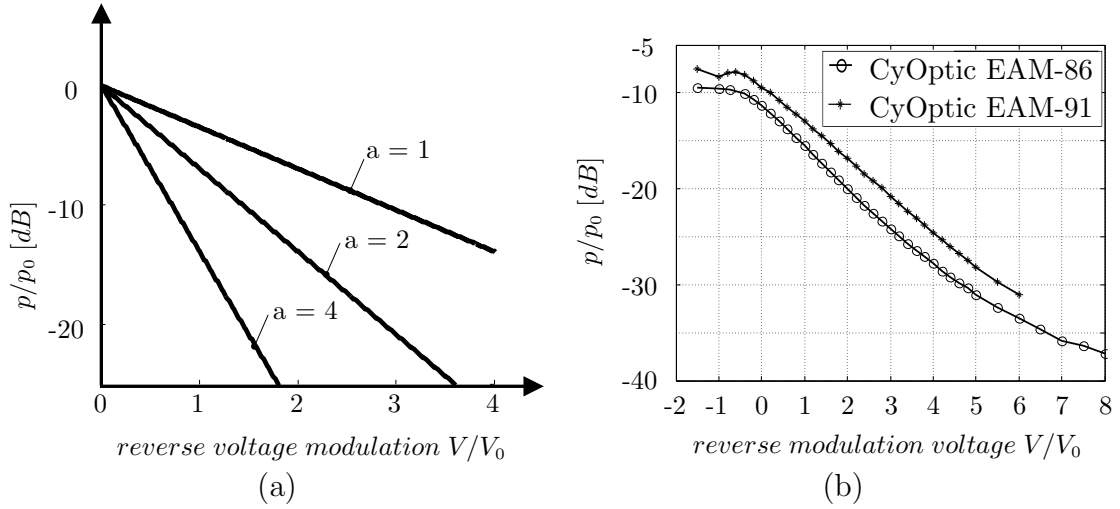


Figure 3.4: EAM transmission characteristic: Plot (a) shows Eq. 3.10 for different technological parameters a ; (b) represents the measured transmission characteristic of optical modulators CyOptic EAM-86 and CyOptic EAM-91.

voltage than bulk EAMs (with smaller a) to reach high power extinction. The extinction ratio is defined as

$$\zeta = 10 \log \left(\frac{p_{\max}}{p_{\min}} \right) [dB], \quad (3.11)$$

where $p_{\max} = p_0$ and p_{\min} are the maximum and the minimum power transmission respectively. Equation 3.10 implies that a high power extinction ratio can be reached when a sufficiently large modulation voltage is applied to the EAM. Extinction ratio up to 40 dB have been reported in [23, 25].

Figure 3.4 (b) shows the transmission characteristic as function of reverse modulation voltage measured in the laboratory. The measurements have been performed on MQW EAMs (CyOptic EAM-86 and CyOptic EAM-91) and the results are in a good agreement with Eq. 3.10 for the parameter set $a = 4$ and $V_0 = 1$ V.

In this work the EAM is used as time-domain filter. In this context the TF is characterized by:

- D factor (D_{TF}) of the TF function
- extinction ratio ζ_{TF} of the TF function
- misalignment Δt_{TF} of the data signal and TF function
- roll-factor α_{TF} of the TF function
- insertion loss (IL) of the EAM.

D factor

The parameter D_{TF} plays an important role in the context of this work. We also use it to switch from a system without time-domain filtering to a system with TF. Figures 3.5 (a)-(c) explain this switching and the influence of D_{TF} on the time-domain filter function in more detail. Figure 3.5 (a) shows the time-domain filter function $f_{\text{TF}}(t)$ for $D_{\text{TF}} = 1$ (i.e. a duty cycle of 100%), which means that the time-domain filter is switched OFF, hence its transmission is equal to unity, and no filtering is performed. Figure 3.5 (b) presents the case for $D_{\text{TF}} = 3$. The filter function varies with the time. This means the filter is switched ON and time-domain filtering is performed. In the case of $D = 3$ only "weak" time-domain filtering takes place. Figure 3.5 (c) represents the case for $D_{\text{TF}} = 10$, which corresponds to "strong" time-domain filtering since about 90% of the bit duration noise is suppressed.

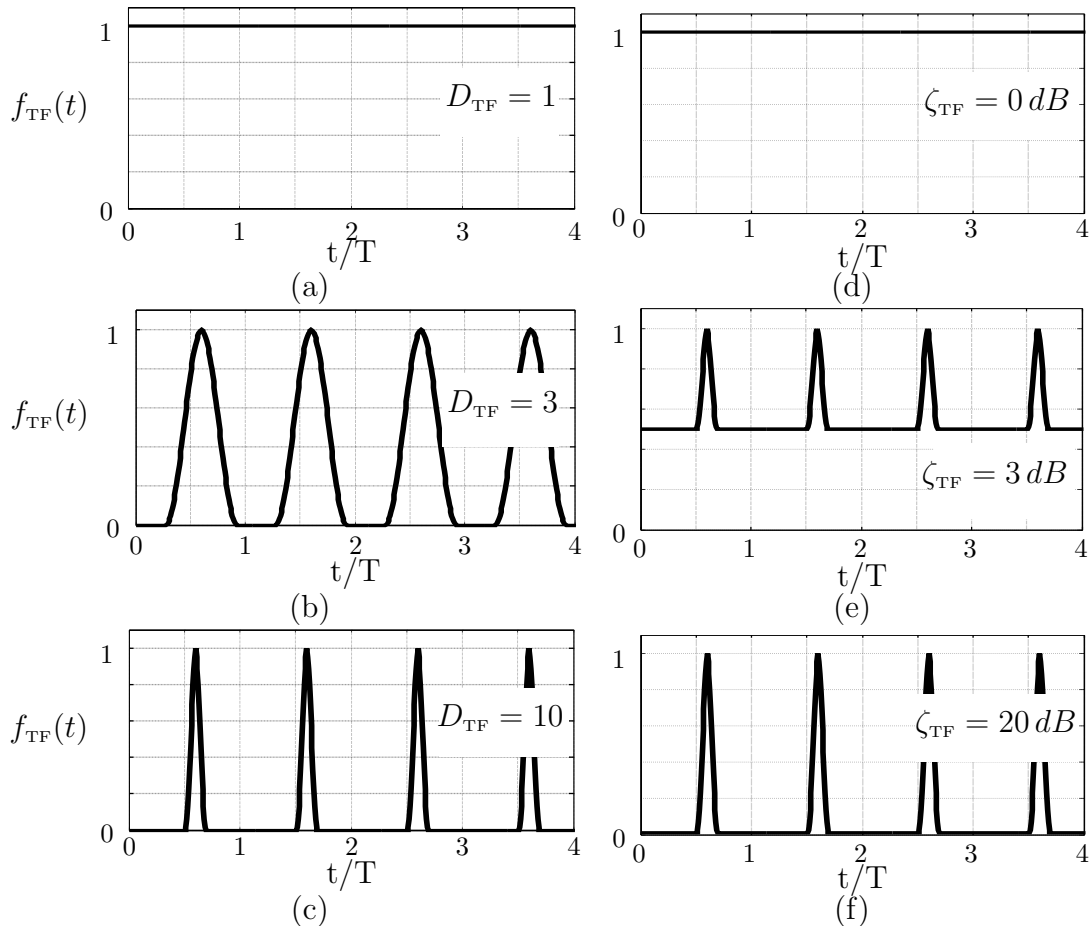


Figure 3.5: (a) -(c) show the influence of D_{TF} on the filter function, in this case $\zeta_{\text{TF}} = 20 \text{ dB}$. Figures (d)-(f) show the influence of the ζ_{TF} on the filter function, in this case $D_{\text{TF}} = 10$. In plot (a) and (d) the TF is switched OFF, while in the other cases the filter is switched ON.

Extinction ratio

The extinction ratio ζ_{TF} of the time-domain filter is defined as

$$\zeta_{\text{TF}} = 10 \log_{10} \left[\frac{f_{\text{TF,max}}}{f_{\text{TF,min}}} \right] \text{ [dB]}, \quad (3.12)$$

where $f_{\text{TF,max}}$ and $f_{\text{TF,min}}$ are the peak and the minimum value of the time-domain filter function $f_{\text{TF}}(t)$ respectively (see Fig. 3.6).

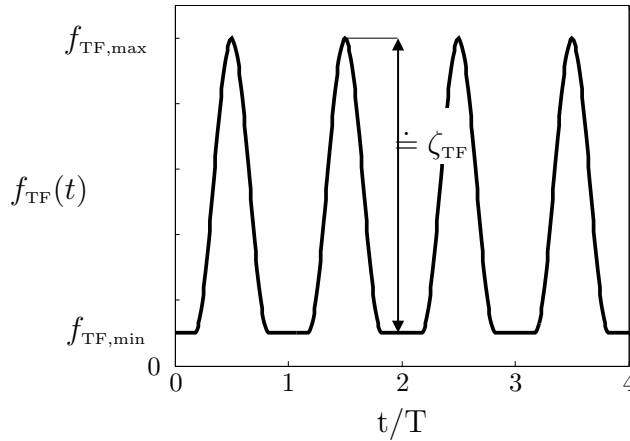


Figure 3.6: Definition of extinction ratio. The two values $f_{\text{TF,max}}$ and $f_{\text{TF,min}}$ are the maximum and the minimum transmission of the time-domain filter function. The logarithmic ratio between $f_{\text{TF,max}}$ and $f_{\text{TF,min}}$ gives the value of ζ_{TF} in dB.

Under ideal conditions, when $f_{\text{TF,min}} = 0$, the *maximum* achievable value for ζ_{TF} is infinity. The *minimum* extinction ratio of 0 dB is reached when $f_{\text{TF,max}} \equiv f_{\text{TF,min}}$. In this case the filter function becomes constant and the TF is switched OFF as shown in Fig. 3.5 (d).

Hence not only D factor but also the extinction ratio can be used to switch the time-domain filter OFF and ON. Figure 3.5 (e) shows the case when the TF is switched ON by using a filter function with $\zeta_{\text{TF}} = 3\text{dB}$. Figure 3.5 (f) shows the filter function for $\zeta_{\text{TF}} = 20\text{dB}$.

Misalignment

In appendix 1 we made the assumption that the TF filter function is perfectly synchronized with the optical data signal. In a real system this assumption does not hold any more. Figure 3.7 (b) visualizes a misalignment Δt_{TF}

$$\Delta t_{\text{TF}} = t_{\max,s} - t_{\max,f}, \quad (3.13)$$

where $t_{\max,s}$ and $t_{\min,f}$ are the time instants when the data signal (solid line) and the TF filter function (dashed line) have their maxima. In the case of perfect synchronization the two maxima coincide and $\Delta t_{\text{TF}} = 0$.

In SimTool it is possible to choose between perfect automatically alignment and manual alignment.

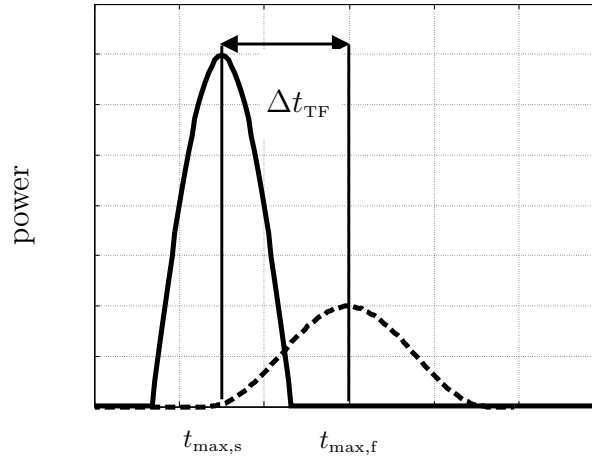


Figure 3.7: Temporal misalignment Δt_{TF} of the TF. The two value $t_{\max,s}$ and $t_{\min,s}$ are the time instant where two functions reach their maxima. The solid line represents the data signal and the dashed stands for the filter function.

Roll-factor

The roll-factor α_{TF} of the TF function is defined exactly in the same way as α was defined for the signal parts in Sec. 3.1.1.

Insertion loss

So far the time-domain filter (TF) has always been considered without insertion loss (IL). Possible insertion losses of the time-domain filter can readily be accounted for by using a reduced effective optical amplifier gain of $G(1 - IL)$. This problem will be discussed in appendix 5 dealing with the measurements.

3.2.4 Photodiode and detection electronics

After time-domain filtering, the data signal is detected by a PIN photodiode. The PIN photodiode performs the conversion of optical power into an electrical current, mathematically described by a square law operation.

In this work the bandwidth of the photodiode can be assumed to be infinity, as it is much bigger than the electrical bandwidth of all following electrical devices (e.g transimpedance amplifier, electrical lowpass filter, cables, BER tester). In our experiments, the bandwidth of the photodiode is about 40 GHz and electrical filter bandwidth ranges up to 10 GHz. Typical sensitivities of conventional photodiodes are about $S = 0.6 A/W$ [19]. A low-noise wide-band transimpedance amplifier is used to transform the weak photo current into a signal voltage necessary for reliable data detection. The entire impulse response of the detection electronics is called $h(t)$ and is determined mainly by the electrical lowpass filter. The response is normalized as [?]

$$\int_{-\infty}^{+\infty} h(t) dt = H(0) = 1 \quad (3.14)$$

In `SimTool` two different filters type are implemented: (a) a first-order RC low pass filter and (b) a fifth-order Bessel filter.

The impulse responde of the RC filter is

$$H_{\text{LF}}(f) = \frac{1}{1 + j\pi f/2B'_e} \quad (3.15)$$

where B'_e denotes the filter power equivalent width [19], being defined as

$$B'_e = \int_0^{+\infty} |H(f)|^2 df. \quad (3.16)$$

Fifth-order Bessel filters (BF) are widely used in optical receivers, since they produce only overshoot. They have the filter transfer function

$$H_{\text{BF}}(s) = \frac{945}{s^5 + 15s^4 - 105s^3 - 420s^2 + 945s + 945}, \quad (3.17)$$

where s stands for the complex variable of the Laplace transform [11, 26].

The impulse responses of a RC filter and a 5th-order Bessel filter are shown in Fig. 3.8 (a) and (b), respectively.

3.3 Limitations of SimTool

The simulation bandwidth (SBW) is defined as the frequency range where correct simulations results are obtained. Ideally the SBW should be infinite. Obviously, this is not possible because of computational constraints of the program.

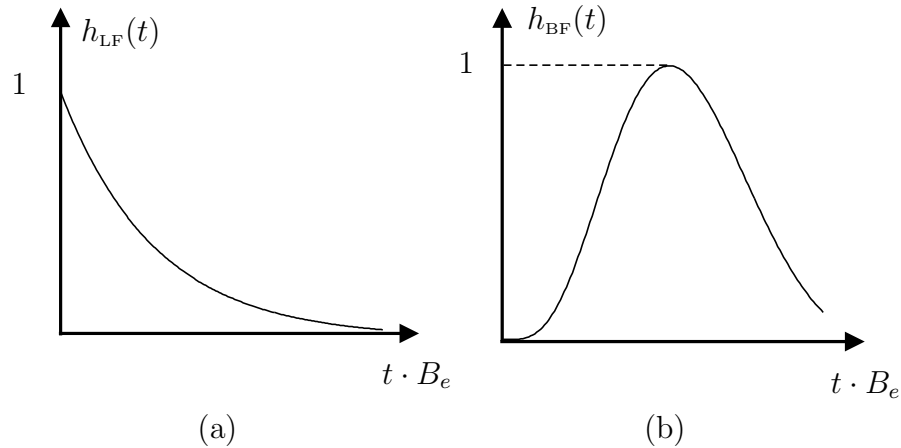


Figure 3.8: Electrical filters: Electrical impulse response of a RC filter (a) and a Bessel filter of 5th-order (b) as function of the time-bandwidth product. The impulse responses are normalized to 1.

The limits in `SimTool` due to the SBW are connected with the modelling of ASE noise and the value of the optical filter bandwidth (OFBW).

We have already mentioned that the ASE noise is modelled in `SimTool` as complex Gaussian white noise. Therefore the value of ASE noise density is constant in the frequency domain and its bandwidth is infinite. The optical filter bandwidth is a simulation parameter. In each simulation a certain value is assigned to this parameter. Hence, the OFBW can be smaller or larger than the SBW. The two cases are indicated in Fig. 3.9 and 3.10, respectively.

Figure 3.9 shows the case where the OFBW is smaller than the SBW. In this case the SBW limits the amount of noise considered in the simulation and the OFBW determines the amount of noise passing the optical filter. The simulation yields a correct result.

The opposite case is shown in Fig. 3.10. For large values of OFBW the SBW limits the bandwidth of the noise taken into account. This results in wrongly calculated receiver sensitivities.

Finally, Fig. 3.11 shows a typical simulation where we obtained wrong results for large OFBW. This simulation analyzes the performance of the sensitivity in an optically preamplified DD receiver when the optical filter bandwidth is changed from $10 R$ to $10^5 R$. As long as the optical bandwidth is smaller than the simulation bandwidth (indicated by "inside of SBW") the sensitivity is calculated correctly. Increasing the OFBW reduces the sensitivity due to the increased amount of noise. But when the OFBW exceeds the SBW, the program does not take into account the noise correctly and the calculated sensitivity is not correct.

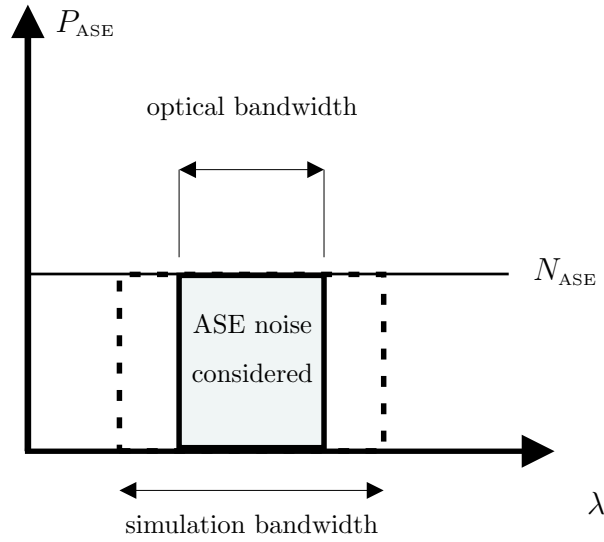


Figure 3.9: Situation when the optical filter bandwidth is smaller than the simulation bandwidth; the noise inside the simulation bandwidth is correctly considered.

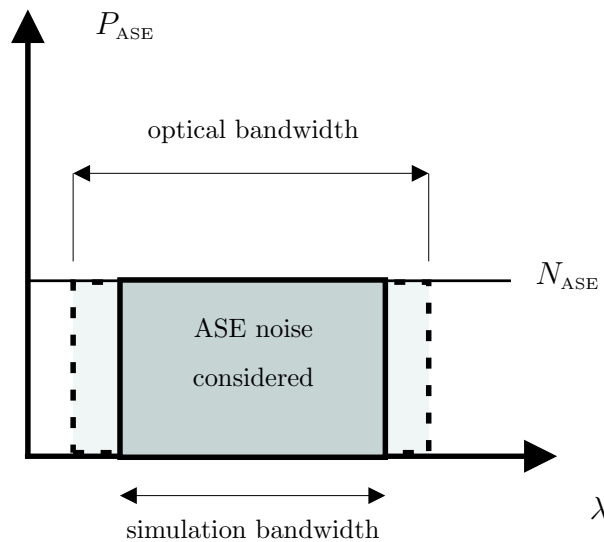


Figure 3.10: Case where the optical filter bandwidth is larger than the SBW; this would yield wrong simulation results.

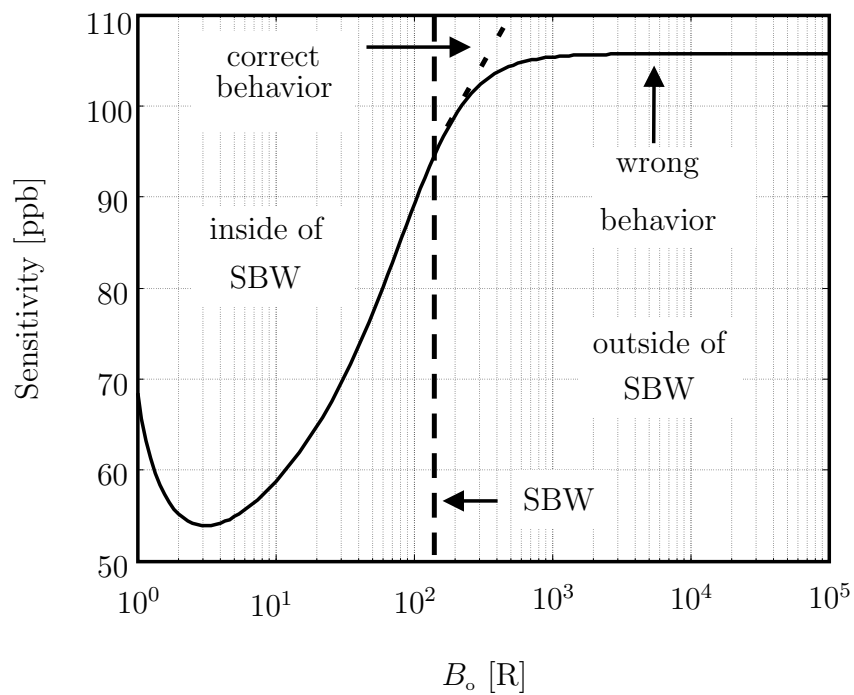


Figure 3.11: Simulation results: the sensitivity is plotted as function of the optical filter bandwidth. On the left side, indicated by "inside of SBW", the calculated sensitivity is correct. On the right side, denoted by "outside of SBW", the solid line gives wrong results. (The correct result would be those indicated by the dashed line).

Chapter 4

Simulation results

This appendix presents the simulation results obtained with `SimTool` modelling an optically preamplified direct-detection receiver employing time-domain filtering. The time-domain filter is placed between the optical bandpass filter and the photodiode (see Fig. 1.3). The aim of this appendix is to study the influence of the main optical transmitter and receiver parameters on the receiver sensitivity. In particular, we will analyze the role of RZ factor D and the roll-off factor α of the data signal, the D_{TF} factor and roll-off factor α_{TF} of the TF function, the extinction ratio ζ_{TF} of the TF function, the electrical bandwidth B_e , the optical bandwidth B_o , and the misalignment Δt_{TF} of the TF function with respect to the data signal.

4.1 Introduction of time-domain filtering

The aim of this section is to study the characteristic of the receiver sensitivity under different conditions, obtained by switching the time-domain filter on and off (compare Sec. 3.2.3).

Figure 4.1 shows the receiver sensitivity expressed in photons per bit [ppb] as a function of D_{TF} (i.e. the duty factor of the time-domain filter) on the left side and as a function of B_o (i.e. the optical bandwidth normalized to the data rate [R]) on the right side. The considered pulse shapes, for both data signal and time-domain filter function are $\cos^2(t)$ -like. Changing of D_{TF} and the optical bandwidth allows us to study the receiver sensitivity of three "different systems": (i) a receiver just using spectral filtering (SF) indicated by the black dot in the figure ("only SF"); (ii) a receiver using both spectral and time-domain filtering, indicated in the middle of the diagram by "SF + TF", and finally (iii) a system only using time-domain filtering (TF), indicated "only TF".

For a better understanding of Fig. 4.1, we consider the case where the TF is switched off (i.e. $D_{\text{TF}} = 1$). The black dot represents a conventional optically preamplified DD receiver without time-domain filtering but with spectral filtering. The receiver sensitivity of that system is about 51 ppb under the assumed conditions. In this case the value of the optical bandwidth is 10 R and the duty cycle of the optical data signal is 10 %. When switching on the TF by increasing D_{TF} we deal with a system of type (ii). Figure 4.1 shows that with increasing D_{TF} , the sensitivity improves. The sensitivity improve-

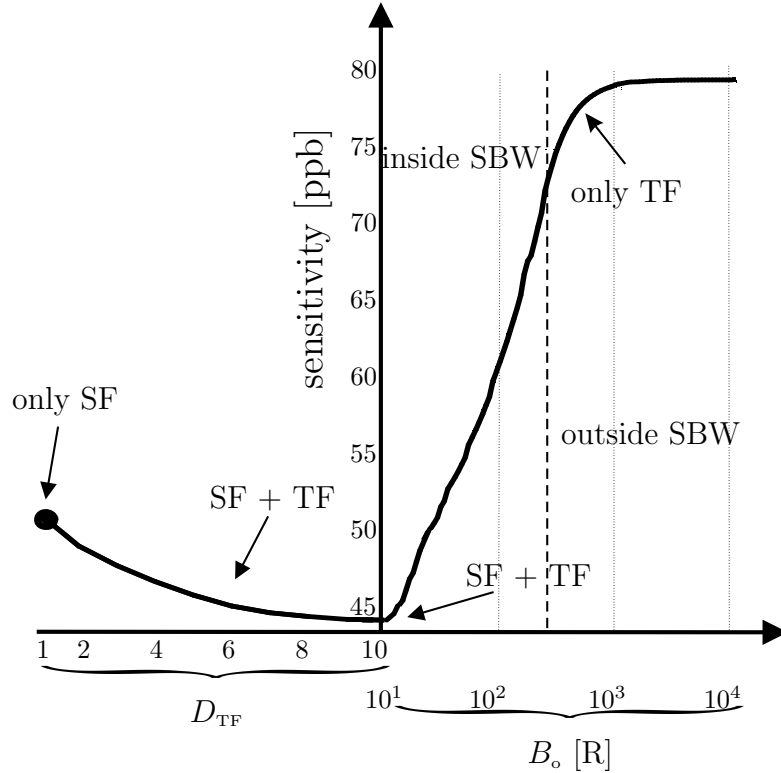


Figure 4.1: Receiver sensitivity as a function of D_{TF} and B_o for the case of $\cos^2(t)$ -like pulses. On the left side the D factor D_{TF} is varied from 1 to 10, while the optical bandwidth is fixed at 10 R. On the right side the optical bandwidth is widened and D_{TF} is 10. The value of the simulation bandwidth (SBW) is 256 R.

ment can be expressed as a gain due to TF and it is denoted by the symbol g_{TF} . The gain is proportional to the noise eliminated by time-domain filtering. Since noise is suppressed for a time period of $1 - d_{TF}$ ($d_{TF} = \text{duty cycle} = 1/D_{TF}$) during a bit slot T as shown in Fig. 4.2, the gain is proportional¹ to $1 - d_{TF} = (D_{TF} - 1)/D_{TF}$. Therefore the absolute improvement in receiver sensitivity increases with higher D_{TF} factors, but the relative improvement decreases. Hence, "moderate" time-domain filtering (e.g. $D_{TF} = 2.5$) yields a reasonable gain, but "strong" TF (e.g. $D_{TF} > 10$) does not improve the sensitivity any more. The gain approaches an asymptotical limit for large values of D_{TF} . Figure 4.1 shows that the maximum sensitivity of 43 ppb is reached when $D_{TF} = 10$. This corresponds to a gain of 8 ppb.

For system (iii) strong TF ($D_{TF} = 10$) is performed and the spectral filter is slowly "switched off" by widening the optical bandwidth until it becomes broad enough to be considered infinite compared to the ASE bandwidth. This is equivalent to a system without a spectral filter. The sensitivity worsens with increasing optical bandwidth B_o due to increased noise as shown in Fig. 4.1. Hence, a time-domain filter without any spectral filtering cannot efficiently suppress noise. The employment of a TF becomes

¹This is only valid under the assumption $D_{TF} < D$.

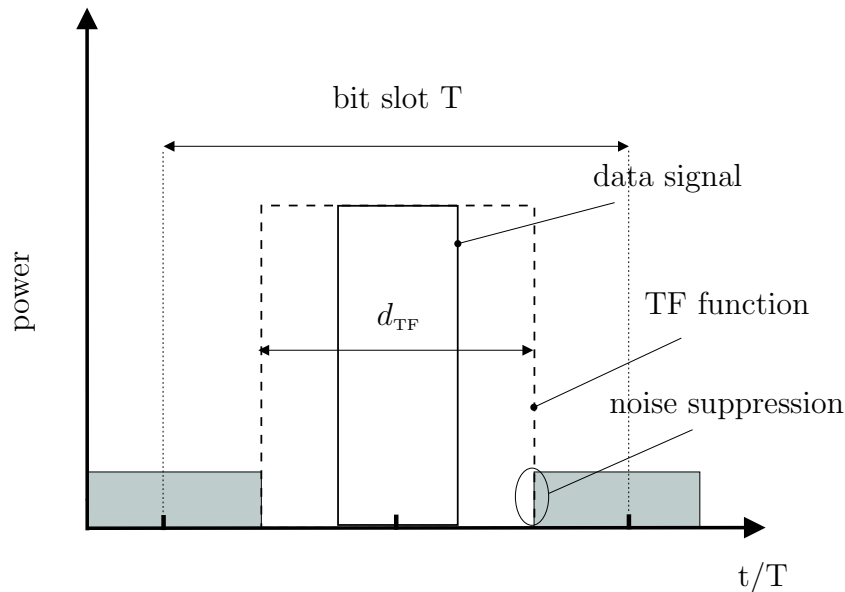


Figure 4.2: Explanation of the influence of the duty cycle d_{TF} on the gain g_{TF} . The dashed line represents the TF filter function, while the solid line is the data signal.

only useful in combination with SF. Note that the calculated sensitivity for optical bandwidths B_o being larger than the Simulation Bandwidth (SBW) is not correct as explained in Sec. 3.3.

Figure 4.3 shows the same simulation as Fig. 4.1 but for the case of rectangular pulse shapes. The absolute gain g_{TF} is larger than for the case of $\cos^2(t)$ -like pulses. This effect will be explained in the next section. However, the absolute sensitivity is worse for rectangular pulse shapes since the pulses are spectrally broader than $\cos^2(t)$ -like pulses and spectrally broader optical filters have to be used [11],

Finally, Fig. 4.4 shows the sensitivity with TF, as it depends on the value of the TF extinction ratio ζ_{TF} (dashed line) and as a function of the TF duty factor D_{TF} (solid line).

Figure 4.4 also shows that $D_{TF} = 10$ (with $\zeta_{TF} = 18 \text{ dB}$) and $\zeta_{TF} = 18 \text{ dB}$ (with $D_{TF} = 10$) are sufficient to maximize the receiver sensitivity. Larger values of these parameters ($D_{TF} > 10$ or $\zeta_{TF} > 18 \text{ dB}$) do not yield additional gain.

4.2 Influence of duty cycle and pulse shape on receiver sensitivity

So far we have only considered the change of D_{TF} while keeping constant the value of D of the data signal. In the following we analyze the interaction of the two D factors. Particularly, we want to find out if there is an optimum combination of D and D_{TF} yielding maximum receiver sensitivity. To study this problem we performed simulations

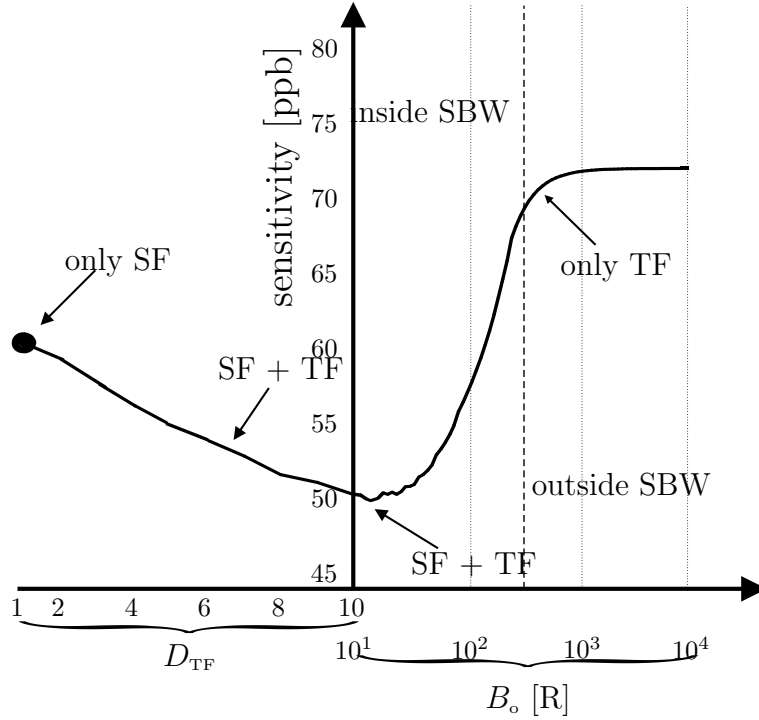


Figure 4.3: Receiver sensitivity as a function of D_{TF} and B_o for the case of rectangular pulses. On the left side the D factor D_{TF} is varied from 1 to 10, while the optical bandwidth is fixed at 10 R. On the right side the optical bandwidth is widened and D_{TF} is 10. The value of the simulation bandwidth (SBW) is 256 R.

by varying D and D_{TF} simultaneously. The results will be expressed in terms of sensitivity penalties (see Eq. ??).

The analysis of the receiver sensitivity as a function of the two D factors is divided in three parts: (i) firstly, we analyze the interaction of D and D_{TF} by using rectangular pulse shapes; (ii) secondly, we consider the case of $\cos^2(t)$ -like pulses for both data signal and time-domain filter function, and finally (iii), we draw the conclusions.

Figure 4.5 shows the sensitivity penalty in dB when both pulse shapes are rectangular. The figure may be divided into three parts, which give the conditions to determine the optimum couple of D factors.

Firstly, we point out the area delimited by the relation $D < D_{TF}$ (indicated in Fig. 4.5 by (A)). In this case the duty cycle of the time-domain filter function is smaller than the duty cycle of the data signal. The receiver sensitivity degrades with increasing D_{TF} since signal energy is cut by the multiplication of the data signal and the time-domain filtering function. This situation is shown in Fig. 4.6, where the solid and dashed line are the data signal and the TF filter function respectively. The grey area represents the amount of signal energy being cut. This consideration leads to the requirement

$$D \geq D_{TF} \quad (4.1)$$

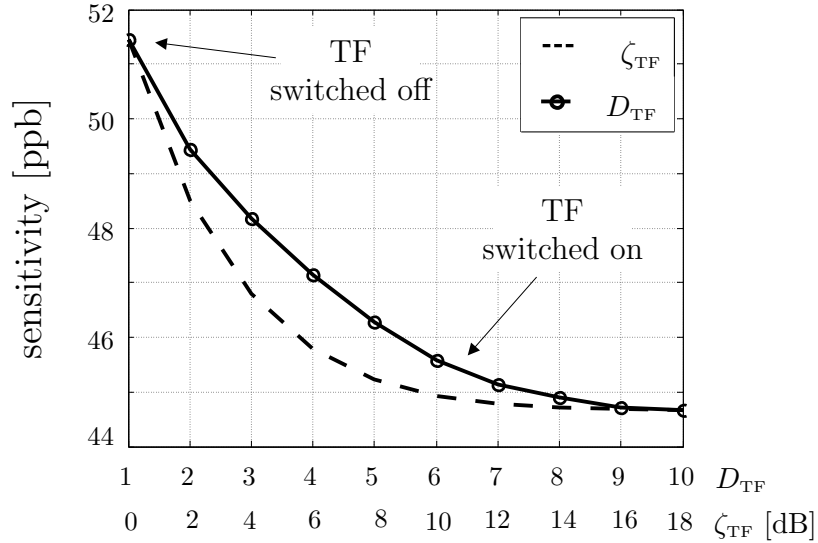


Figure 4.4: Influence of varying either the duty D factor D_{TF} (solid line) or the extinction ratio ζ_{TF} (dashed line) on the receiver sensitivity. For the case of solid line the extinction ratio was $\zeta_{TF} = 20$ dB, for the dashed line the duty D factor was $D_{TF} = 10$.

to achieve good sensitivity.

Secondly, we consider the case when $D > D_{TF}$, indicated by (B) in Fig. 4.7. In this case only noise suppression due to TF takes place. The situation is the same as shown in Fig. 4.2, where the solid and dashed line are the data signal and the TF filter function respectively. The TF filter function reduces noise without cutting signal energy.

Thirdly, there is the case of $D \simeq D_{TF}$, indicated by the thick solid line (C). It is evident that, for the case of rectangular pulse shapes, the optimum values of receiver sensitivity are found when $D = D_{TF}$ since maximum noise suppression takes place without signal cutting (see Fig. 4.8 (a)). In this case the two pulses completely overlap and noise between the bits is eliminated to a maximal degree.

We conclude that, in case of the rectangular pulse shape, the maximum sensitivity is achieved when

$$D \equiv D_{TF}. \quad (4.2)$$

Under this condition the maximum gain due to TF is about 0.8 dB.

Figure 4.7 shows the same simulation as Fig. 4.5 but for the case of $\cos^2(t)$ -like pulses. The simulation results are different from those obtained with rectangular pulses, since $\cos^2(t)$ -like TF pulses always cause a reduction of the signal energy. The multiplication of the data signal with the $\cos^2(t)$ -like pulses always attenuates the signal power except for the instant of maximum transmission. This situation is shown in Fig. 4.8 (b) for the case $D = D_{TF}$. This signal energy cutting causes a shift of the maximum sensitivity towards larger value of D (compared to rectangular pulses) as indicated by the thick line in Fig. 4.7. Optimum performance is now obtained for

$$D > D_{TF}. \quad (4.3)$$

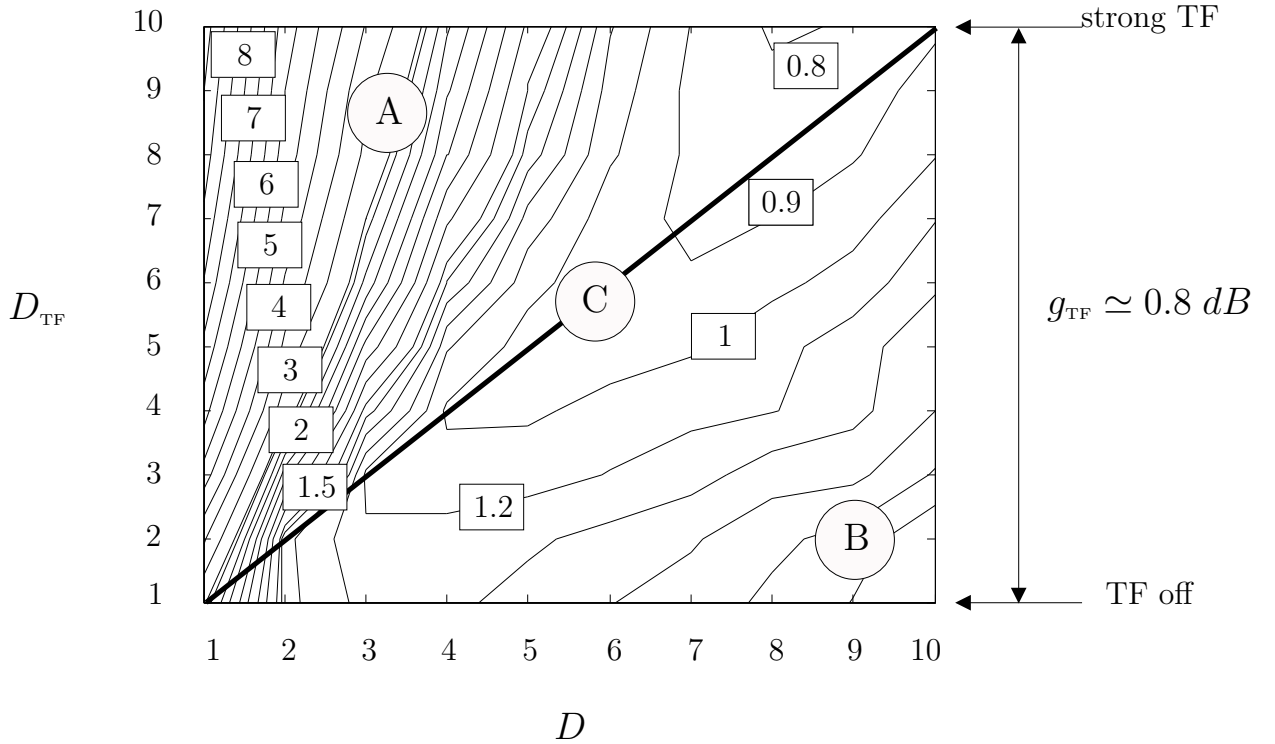


Figure 4.5: Contour lines of receiver sensitivity relative to the quantum limit (41 ppb) [dB] as function of D and D_{TF} for rectangular pulses. The diagram may be divided in three parts: (A) $D < D_{\text{TF}}$, noise + signal energy are both present; (B) $D > D_{\text{TF}}$, only noise suppression takes place; (C) is the line of the maximum sensitivity.

The last result comes from a trade-off between maximum noise suppression (provided when $D = D_{\text{TF}}$) and minimal energy reduction ($D > D_{\text{TF}}$). The gain due to TF is 0.6 dB. This gain is smaller than the gain in case of rectangular pulses.

Finally, we draw the conclusions.

- The optimum pulse shapes of the time-domain filter function is found to be rectangular since this does not cut any signal energy.
- The optimum shape of the data signal is with such pulses a $\cos^2(t)$ since better signal is reached [11] pulses.

The optimum constellation of the D-factors depends on the signal shapes:

- $D_{\text{TF}} \equiv D$ for rectangular pulses
- $D_{\text{TF}} < D$ for $\cos^2(t)$ -like

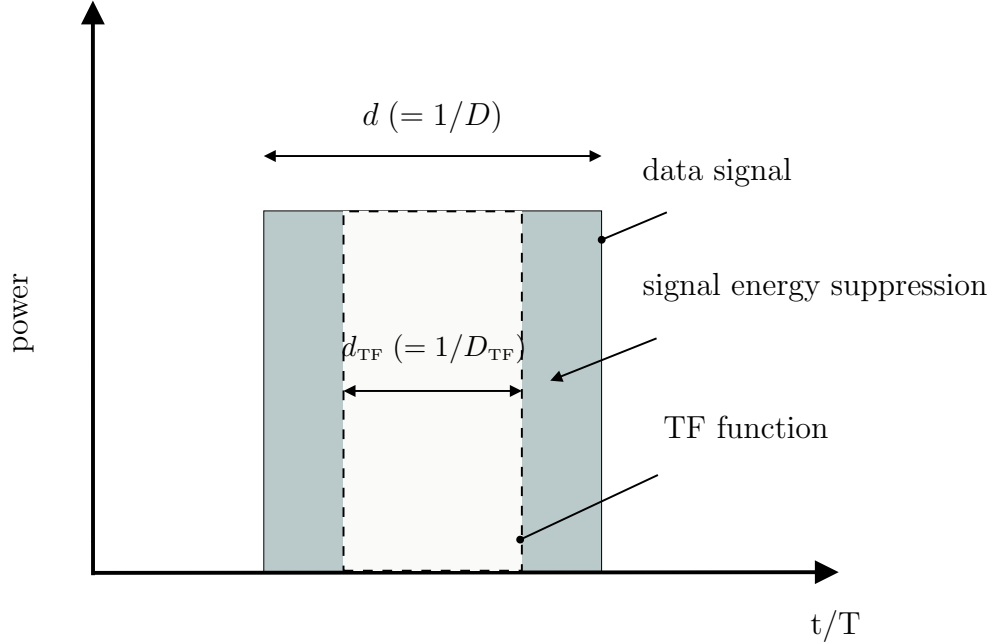


Figure 4.6: $D < D_{\text{TF}}$: The data signal energy (solid line) is suppressed by the time-domain filter function (dashed line).

4.3 Influence of the electrical bandwidth

The improvement of the receiver sensitivity due to time-domain filtering strongly depends on the electrical filter bandwidth of the detection chain. This section gives (i) the reasoning why the time-domain filtering gain vanishes with large electrical bandwidth, (ii) shows that only ASE-ASE beat noise is suppressed by the time-domain filter but not signal-ASE beat noise, and (iii) presents comprehensive simulations of the combined influence of the electrical bandwidth and the duty cycles on the receiver sensitivity penalty.

Figure 4.9 (a) shows the electrical mean of the detected signal at a receiver without time-domain filtering. The corresponding bit sequence is 01101 and the optical/electrical bandwidths are 2/0.6 times the data rate. Figure 4.9 (b) just indicates that the standard deviation $\sigma_{\text{ASE,ASE}}$ of the ASE-ASE beat noise is constant in time. Figure 4.9 (c) shows the standard deviation $\sigma_{\text{sig,ASE}}$ of the signal-ASE beat noise and the standard deviation of the total noise

$$\sigma = \sqrt{\sigma_{\text{ASE,ASE}}^2 + \sigma_{\text{sig,ASE}}^2}, \quad (4.4)$$

where we assumed that the thermal noise is negligible [15]. In contrast, Fig. 4.10 shows the electrical mean and the standard deviations of noise for a receiver employing time-domain filtering. The ASE-ASE beat noise (see Fig. 4.10 (b)) becomes time dependent, i.e. it is "modulated" by the time-domain filter at a rate equal to the data rate R . This modulated ASE-ASE noise is lowpass filtered by the electrical filter of the detection chain.

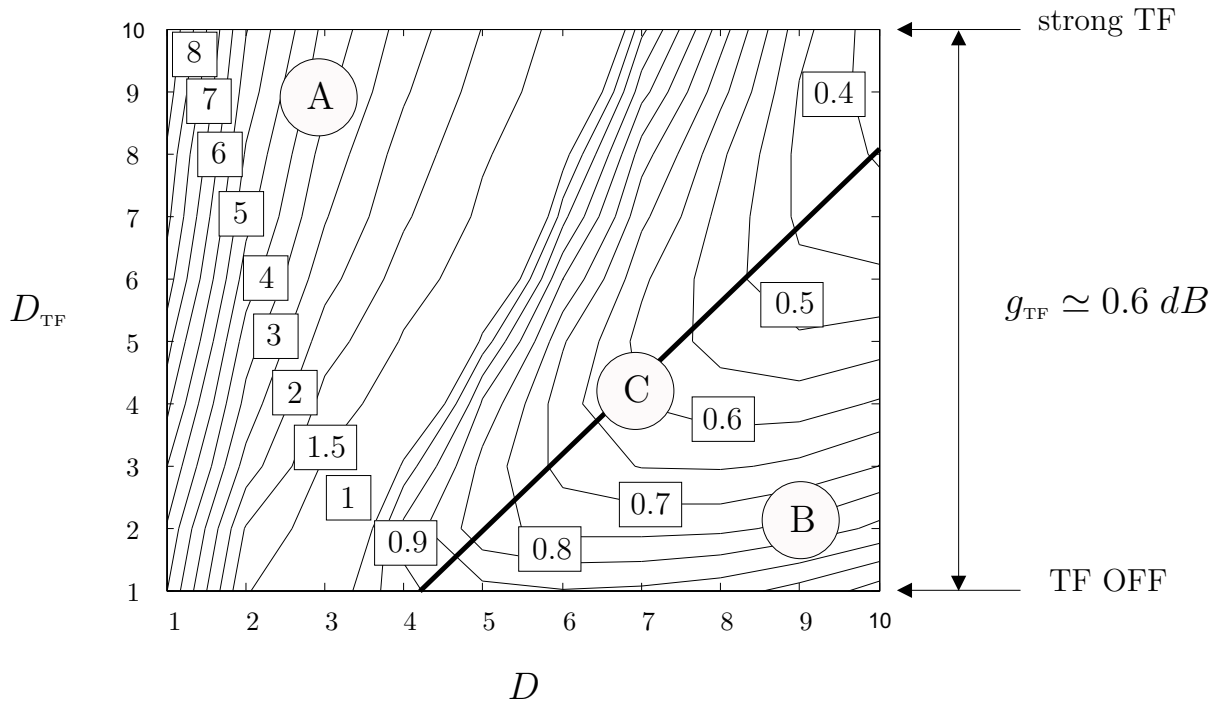


Figure 4.7: Contour lines of receiver sensitivity relative to the quantum limit (41 ppb) [dB] as function of D and D_{TF} for $\cos^2(t)$ -like. The diagram may be divided into three parts: (A) when $D < D_{TF}$, characterized by noise + cutting signal degradation; (B) where $D > D_{TF}$, characterized by noise suppression only and (C) with D_{TF} a little bit smaller than D , where the sensitivity penalty is minimal.

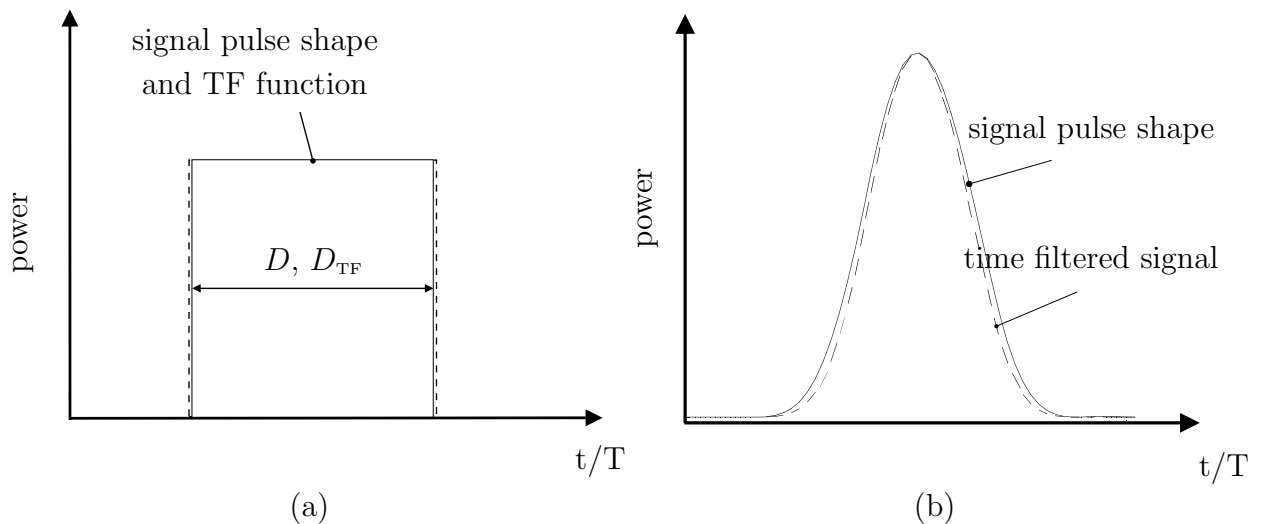


Figure 4.8: Plot (a) shows the case of rectangular shapes for both the signal and the TF. In this case filtering does not change the signal shape. Plot (b) shows the case of $\cos^2(t)$ -like shapes; the two signals have identical level only at the pulse center. For other points a $\cos^2(t)$ -like TF introduces signal energy reduction.

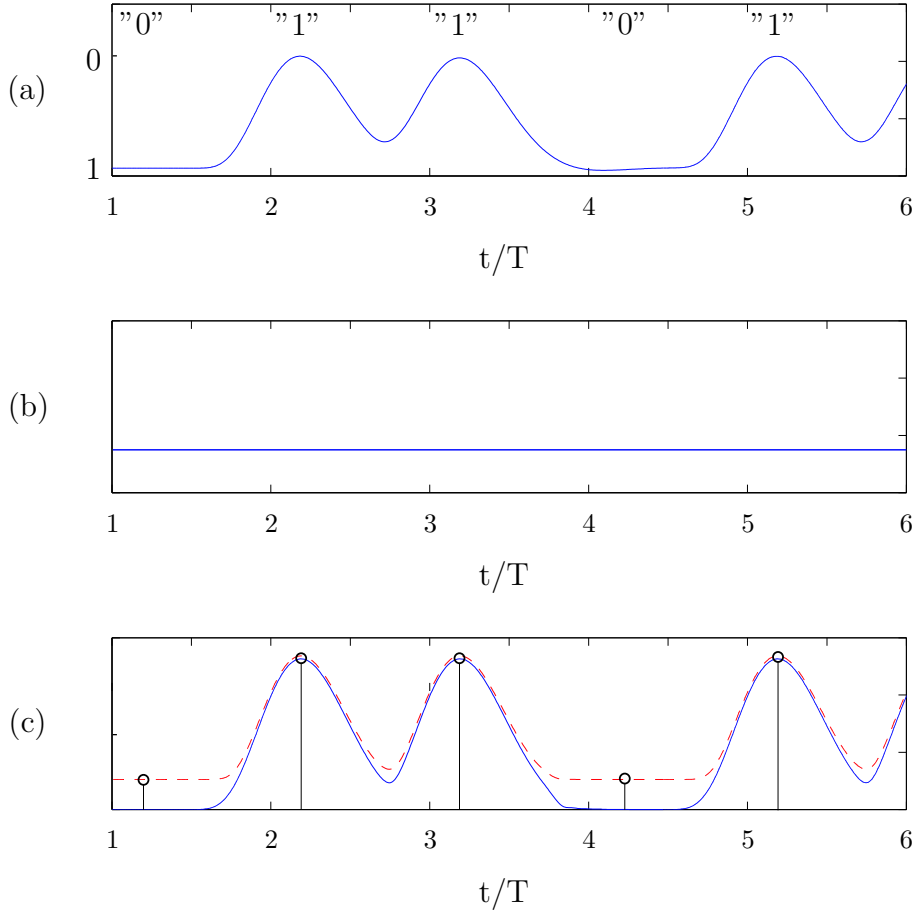


Figure 4.9: Plot (a) shows the electrical mean of the detected signal at a receiver without time-domain filter. Plot (b) indicates the standard deviation $\sigma_{ASE,ASE}$ of the ASE-ASE beat noise. Plot (c) depicts the standard deviation $\sigma_{sig,ASE}$ of the signal-ASE beat noise (solid line) and the standard deviation of the total noise (dashed line).

Therefore, if an electrical bandwidth being broad compared to the used data rate, the ASE-ASE noise can pass the filter unchanged. In contrast, if a small electrical filter bandwidth is used ($B_e < R$), the lowpass reduces the noise power as a result, at the sampling time instants the ASE-ASE noise - and consequently also the total noise - is reduced yielding improved receiver sensitivity. *At the sampling instants* the signal-dependent signal-ASE beat noise shown in Fig. 4.10 (c) is not affected by the time-domain filter. However, since the time-domain filter suppresses signal and noise between consecutive bits, the signal-ASE noise is also decreased there. Since (i) this signal-ASE noise reduction is small compared to the ASE-ASE noise reduction and (ii) the reduction occurs only between the bits but not at the sampling instants, it does not influence the receiver sensitivity.

Figures 4.11, 4.12 and 4.13 show the sensitivity penalty [dB] as a function of the D-factor of the time-domain filter function and the data signal for different electrical bandwidths; Fig. 4.11 characterizes a receiver with an electrical bandwidth of $B_e = 10R$. The sensi-

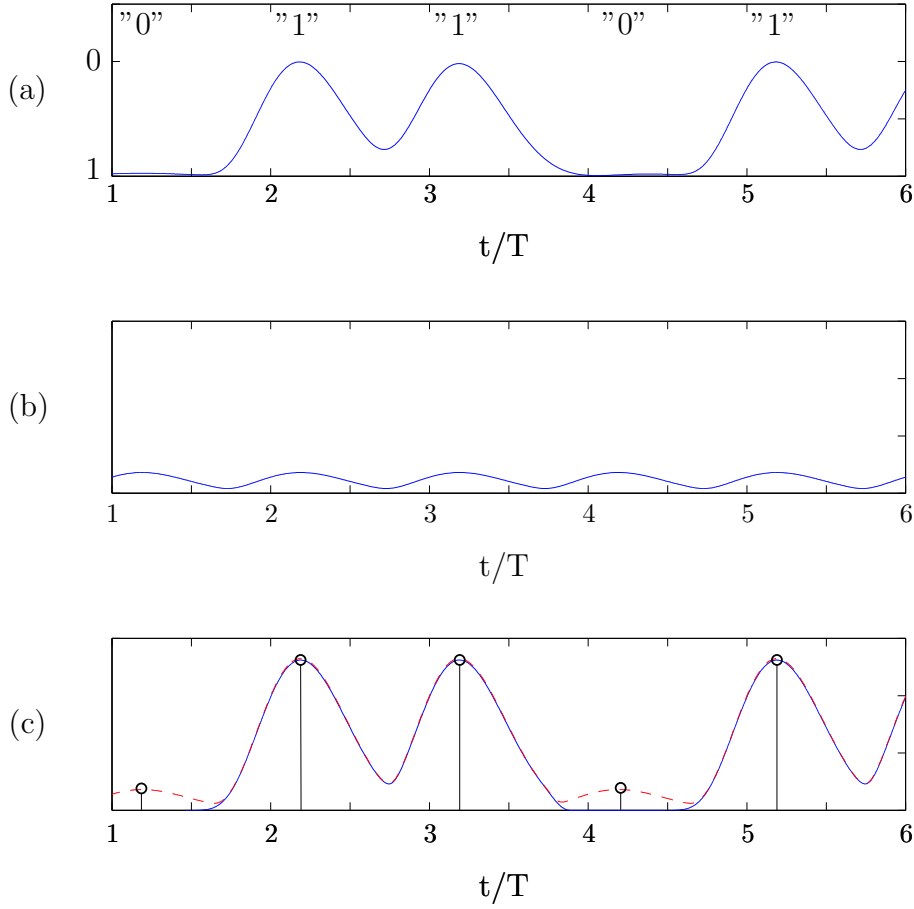


Figure 4.10: Plot (a) shows the electrical mean of the detected signal at a receiver with time-domain filter. Plot (b) indicates the standard deviation $\sigma_{ASE,ASE}$ of the ASE-ASE beat noise. The noise is time modulated by the TF function. Plot (c) depicts the standard deviation $\sigma_{sig,ASE}$ of the signal-ASE beat noise (solid line) and the standard deviation of the total noise (dashed line)

tivity penalty is almost independent of the time-domain filter parameter D_{TF} , i.e. the time-domain filter does not hardly influence the system and it yields a negligible gain of 0.05dB at $D = 10$. This simulation result is in agreement with the explanation for the interplay of the electrical bandwidth and time-domain filtering given above.

For the simulation results in Fig. 4.13 the electrical bandwidth was set to $B_e = 2R$. The receiver sensitivity is influenced by the time-domain filter and yields a gain of 0.3 dB at $D = 10$.

When setting the electrical bandwidth to $B_e = 0.8R$ (see Fig. 4.13), ASE-ASE noise is strongly suppressed by the time-domain filter and a gain in receiver sensitivity of about 0.6 dB can be reached for signals with $D = 10$. Hence, time-domain filtering *only* improves the receiver performance when narrow electrical filtering ($B_e < R$) is performed. Otherwise, time-domain filtering does *not* affect the receiver sensitivity.

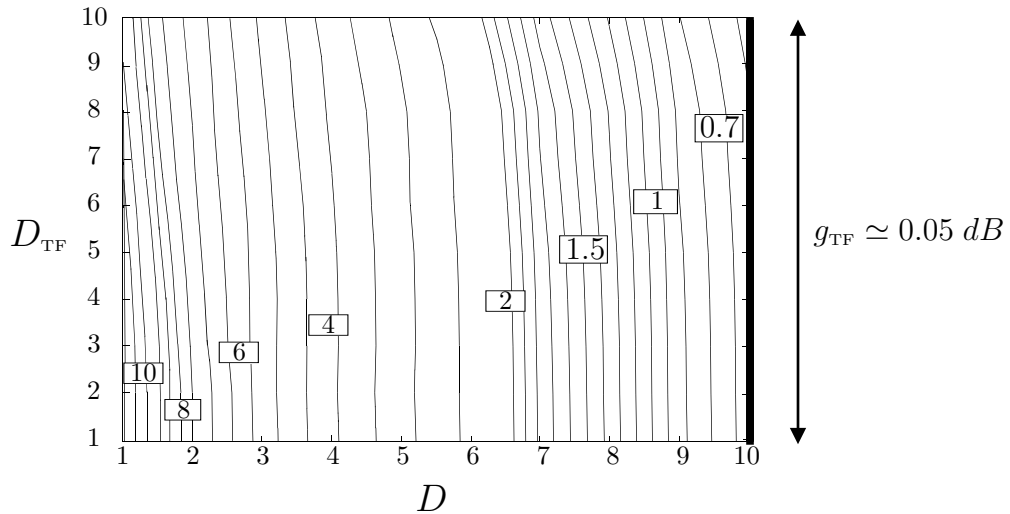


Figure 4.11: Contour lines of receiver sensitivity penalty [dB] as function of D and D_{TF} for $\cos^2(t)$ -like pulses. The value of the electrical filter bandwidth is 10 R. The gain due to the time-domain filtering is negligibly small amounting to 0.05 dB.

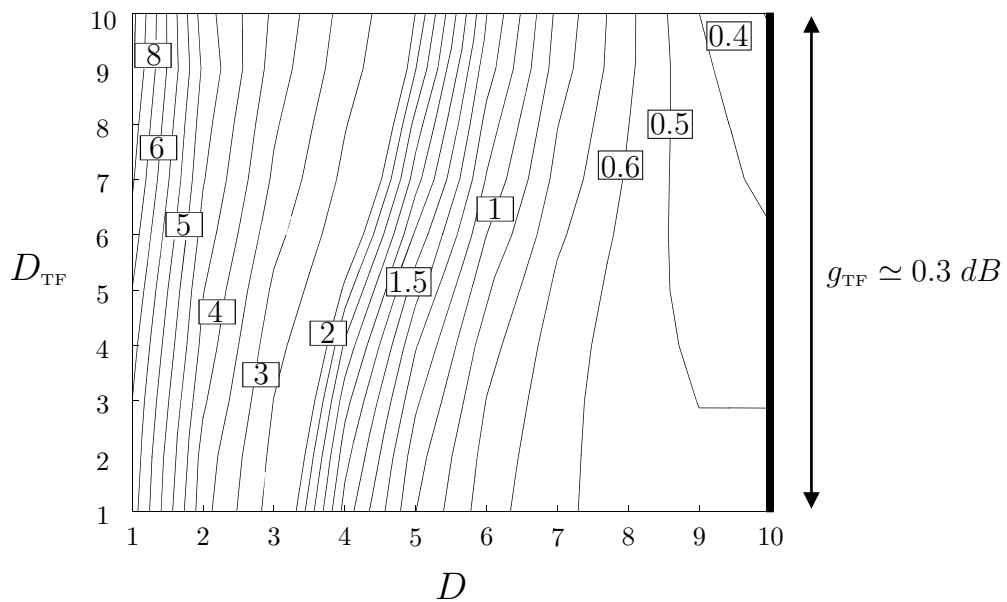


Figure 4.12: Contour lines of receiver sensitivity penalty [dB] as function of D and D_{TF} for $\cos^2(t)$ -like pulses. The value of the electrical filter bandwidth is 2 R. The gain due to the time-domain filtering amounts to about 0.3 dB.

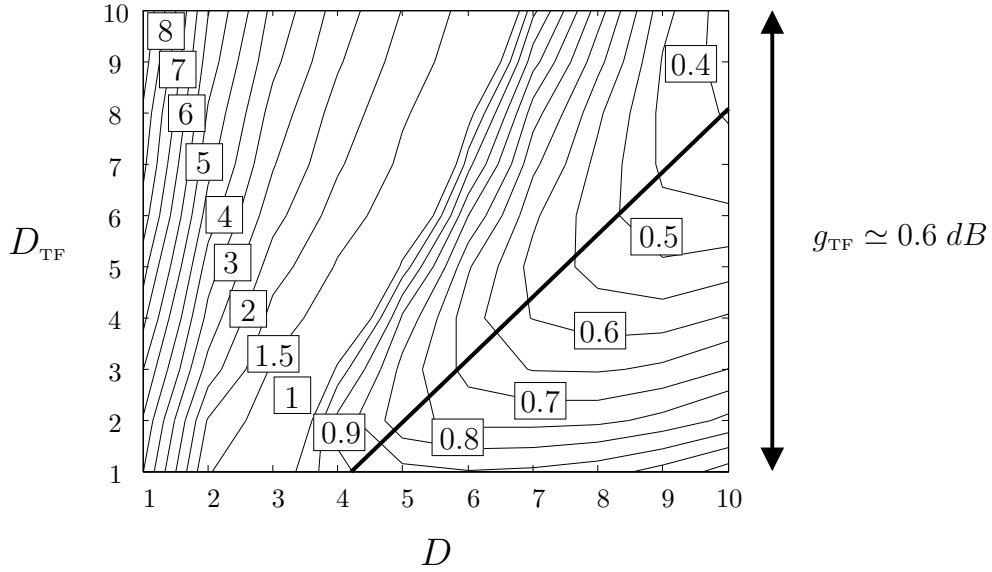


Figure 4.13: Contour lines of receiver sensitivity penalty [dB] as function of D and D_{TF} for $\cos^2(t)$ -like pulses. The value of the electrical filter bandwidth is $0.8 R$. For this value the gain due to the time-domain filter reaches almost the maximum value of about 0.6 dB.

4.4 Influence of extinction ratio on receiver sensitivity

The aim of this section is to analyze the influence of TF extinction ratio ζ_{TF} and the duty factor D_{TF} on the gain obtained by using time-domain filtering. The other simulation parameters are set to their optimum values. This choice allows us to reach the maximum TF gain, which is a necessary condition to analyze the influence of ζ_{TF} on TF gain g_{TF} since we saw that the gain due to TF is only 0.6 dB.

Figure 4.14 shows the receiver sensitivity penalty [dB] as a function of D_{TF} and ζ_{TF} . We consider four cases with fixed extinction ratios at 0 dB, 3 dB, 12 dB and 20 dB (thick lines in the Fig. 4.14). The first line ($\zeta_{\text{TF}} = 0$ dB) represents a system without TF (see Fig. 3.5 (d)), which does not yield any gain due to time-domain filtering. By increasing ζ_{TF} to 3 dB the gain is not negligible any more and becomes $g_{\text{TF}} \approx 0.3$ dB.

When considering the third line at $\zeta_{\text{TF}} = 12$ dB, the system yields almost the maximum value for the gain obtained by using TF. Further increasing the extinction ratio does not increase the gain any more. Therefore a value of 12 dB of extinction ratio is sufficient to have the best system performance. This result will be useful in appendix 6, dealing the measurements: It allows us to perform useful measurements with an extinction ratio of only 12 dB.

As becomes clear from Fig. 4.14, both ζ_{TF} and D_{TF} influence the amount of time-domain filter action. The contour lines resemble hyperboles. To achieve constant sensitivity

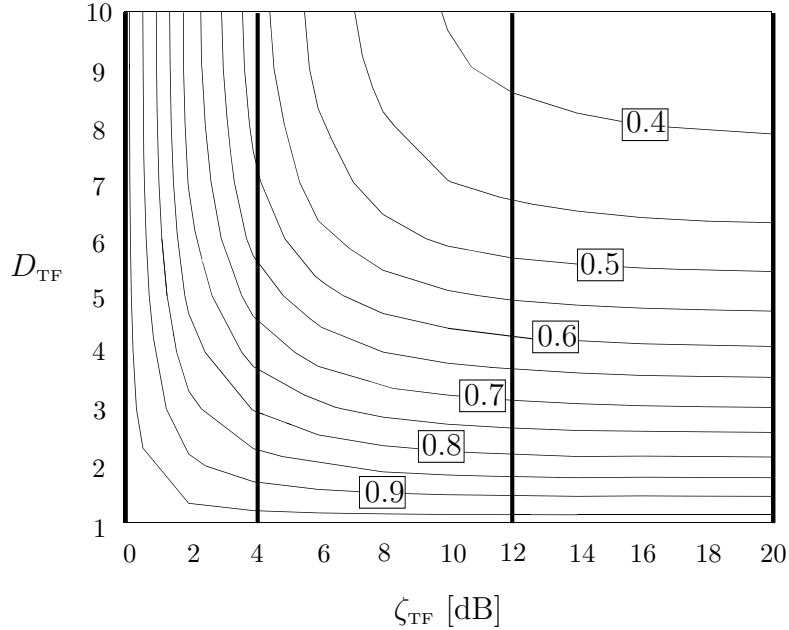


Figure 4.14: Influence of ζ_{TF} and D_{TF} on receiver sensitivity penalty [dB], shown as contour lines for the case $D = 10$. The line at $\zeta_{\text{TF}} = 0$ dB shows a negligible gain due to TF; following the line at $\zeta_{\text{TF}} = 4$ dB one finds a gain of 0.4 dB. For $\zeta_{\text{TF}} = 12$ dB and 20 dB we obtain the maximum TF gain of 0.6 dB.

penalty, the relation

$$\zeta_{\text{TF}} \cdot D_{\text{TF}} = \text{cost} \quad (4.5)$$

must be observed. This is understandable if we recall that the considered parameters give a contribution to noise suppression in different ways (see Sec. 3.2.3). As consequence of this relation we find that a filter with low ζ_{TF} must have higher D_{TF} to reach the same filter action as a system with high ζ_{TF} and low D_{TF} .

4.5 Influence of misalignment on receiver sensitivity

Section 3.2.3 defined the relative temporal misalignment Δt_{TF} of time-domain filtering and the importance of considering it in the analysis of a real optically preamplified DD receiver employing TF. We recall that Δt_{TF} is defined as misalignment of the data signal after the optical bandpass filter and the time-domain filter function. The parameter Δt_{TF} can strongly influence the receiver sensitivity and its study is the topic of this section. Simulations were performed calculating the receiver sensitivity penalty as a function of Δt_{TF} , D_{TF} , and D .

The misalignment range considered was $0 \leq \Delta t_{\text{TF}} \leq 0.3T$. A larger range is not of interest since the receiver sensitivity penalties would become too large. The sign of Δt_{TF} is considered to be positive. A negative sign would provide exactly the same simulation

results. Figure 4.15 shows the case when the optical data signal and time-domain filter function, are not synchronized.

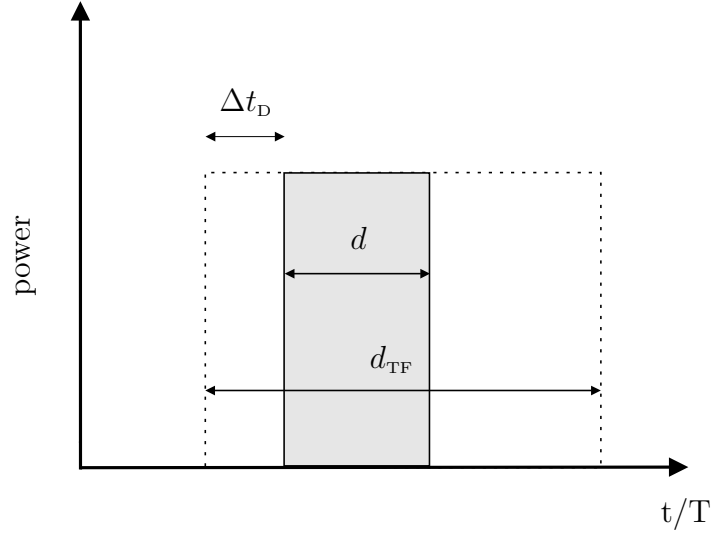


Figure 4.15: Case of desynchronizing when $d_{\text{TF}} > d$. The data signal energy (solid line) is not cut by the multiplication with time-domain filter function (the dashed line).

Equation 3.13 gave the mathematical definition of misalignment. To avoid signal cutting due to temporal misalignment the condition

$$\Delta t_{\text{TF}} \leq \frac{d_{\text{TF}} - d}{2}, \quad (4.6)$$

has to be fulfilled. Equation 4.6 becomes evident when viewing Fig. 4.16. When Δt_{TF} becomes larger than $(d_{\text{TF}} - d)/2$ then strong sensitivity degradation is caused due to signal cutting. Equation 4.6 is only valid when $d_{\text{TF}} > d$ and for positive misalignment. Equation 4.6 further implies that when $d_{\text{TF}} \gg d$, misalignment is less critical. In contrast if $d_{\text{TF}} \simeq d$, the upper limit becomes smaller and hence the influence of misalignment is strong. In case of $d_{\text{TF}} = d$ no misalignment at all is allowed (see Fig. 4.16).

Figure 4.17 shows the receiver sensitivity penalty as a function of D_{TF} and Δt_{TF} . The value of D is kept constant at 10. The contour lines obtained in this simulation confirm Eq. 4.6. When $D_{\text{TF}} = 2$ (corresponding to $d_{\text{TF}} \gg d$) the sensitivity does not deteriorate even for large Δt_{TF} . In contrast, when $D_{\text{TF}} = 10$ we have good system performance only when $\Delta t_{\text{TF}} = 0$.

Figure 4.18 shows a diagram derived by similar simulations as shown in Fig. 4.17. In this plot we only report simulations when $D \equiv D_{\text{TF}}$.

For small D factors, the energy signal cutting due to the misalignment is less pronounced than for the case of large D factors. When D is large even a small Δt_{TF} can produce a drastic reduction of the system performance.

Misalignment Δt_{TF} is a critical issue with time-domain filtering. Clearly, a system which operating at small D factors is less sensitive to misalignment than a system with large D .

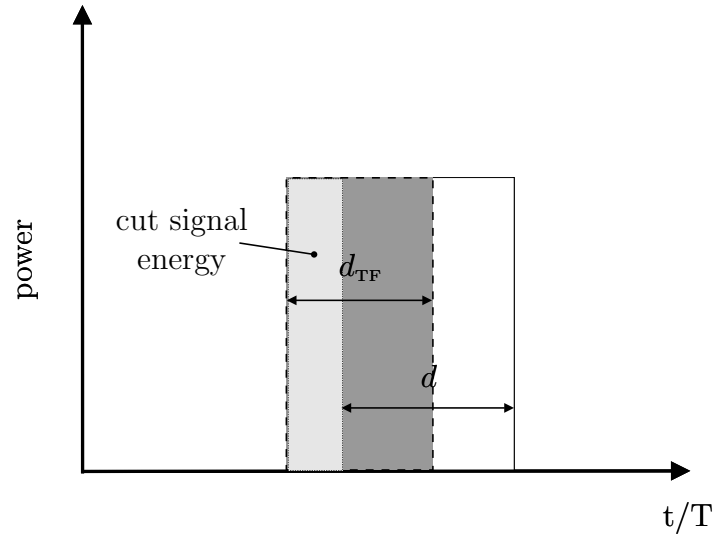


Figure 4.16: Case of temporal misalignment Δt_{TF} in case of $d_{\text{TF}} \simeq d$. The data signal energy (solid line) is partially suppressed by the multiplication with time-domain filter function (dashed line).

As examples, we found a misalignment penalty of $\approx 4.6 \text{ dB}$ for $\Delta t_{\text{TF}} = 0.1$ for the case of $D = D_{\text{TF}} = 10$ and a penalty of $\approx 1.1 \text{ dB}$ for $\Delta t_{\text{TF}} = 0.2$ for the case of $D = D_{\text{TF}} = 3$. These penalties are relative to the perfectly aligned case of $\Delta t_{\text{TF}} = 0$.

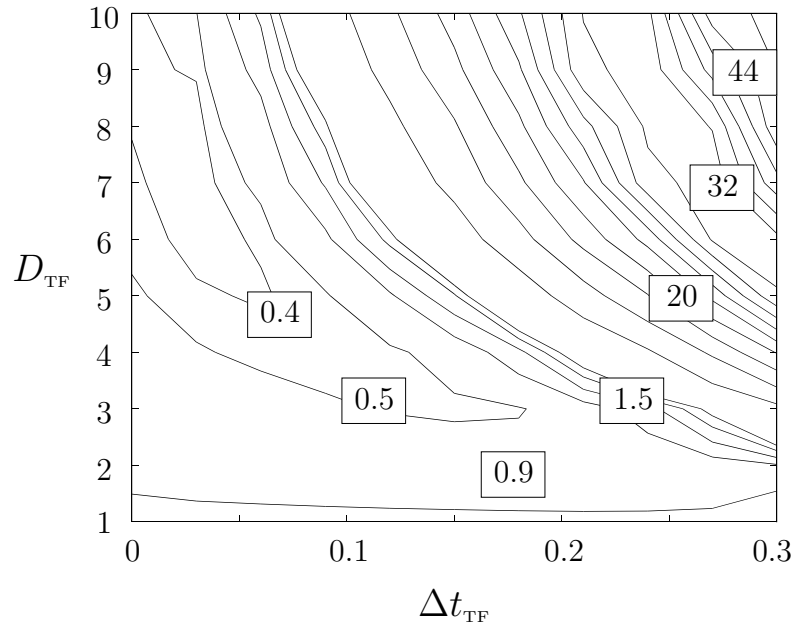


Figure 4.17: Contour lines of receiver sensitivity penalty [dB] as a function of D_{TF} and Δt_{TF} for $D = 10$.

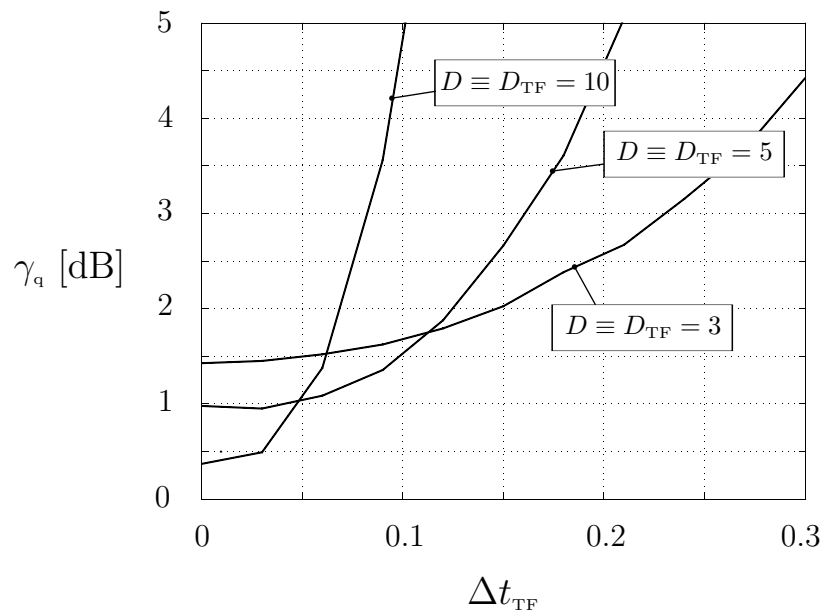


Figure 4.18: Receiver sensitivity penalty [dB] for the case of $D \equiv D_{TF}$ as a function Δt_{TF} .

Chapter 5

Measurements

This appendix presents measurements performed at the optical laboratory of the *Institut für Nachrichtentechnik und Hochfrequenztechnik* of the *Technische Universität Wien* (Austria). The appendix is structured as follows: Firstly, the measurement setup of an optical back-to-back communication system and the generation of the signals used are described. Secondly, sensitivity measurements with and without optical time-domain filtering and by varying the electrical and optical bandwidth are presented. Finally a comparison between measurements and simulations is given. The experiment turn out to be in good agreement with the theory.

5.1 Measurement setup

Figure 5.1 shows the complete system setup for the measurements performed at a data rate of 1 Gb/s. It consists of a transmitter, a receiver, and a circuit to generate driving signals for the transmitter and the time-domain filter. It is also included signal monitoring to visualize optical and electrical signals at various points. In the following context we will always use the mentioned system setup, but the electrical and optical filter bandwidths will be changed.

5.1.1 Transmitter

The transmitter (see Fig. 5.1) used in the experiments consists of

- a tunable semiconductor laser diode
- an electroabsorption modulator (EAM)
- a polarization controller (PC)
- a Mach-Zehnder modulator (MZM)
- a signal pattern generator

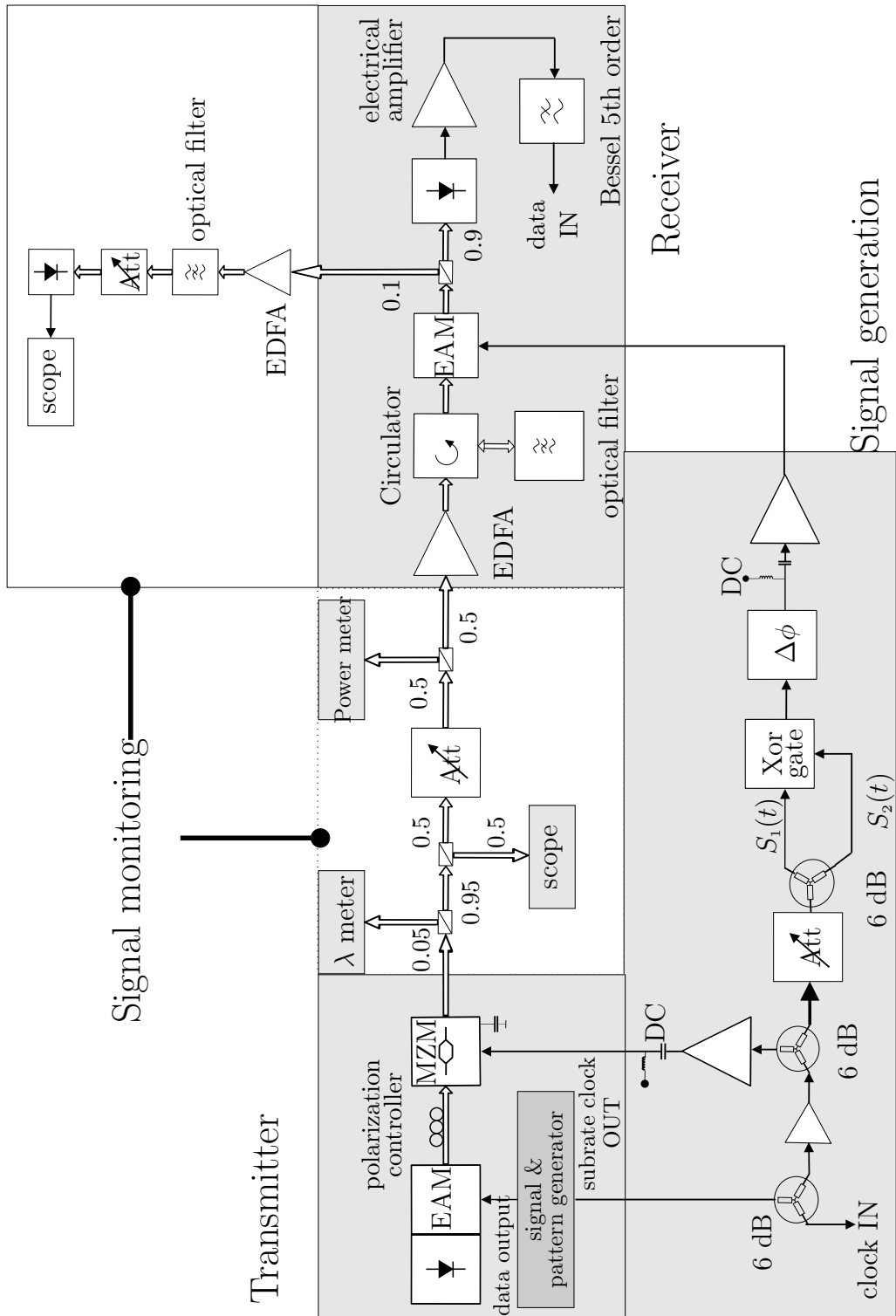


Figure 5.1: System measurement setup employing time-domain filtering at data rate of 1 Gb/s. The system is divided into four parts: transmitter, receiver, driving circuits, and signal monitoring.

In order to be able to measure the influence of time-domain filtering on the receiver sensitivity we had to generate an optical data signal with high D factor. Such a signal is generated by performing a dual-stage modulation. Figure 5.2 (a) shows the modulation scheme used.

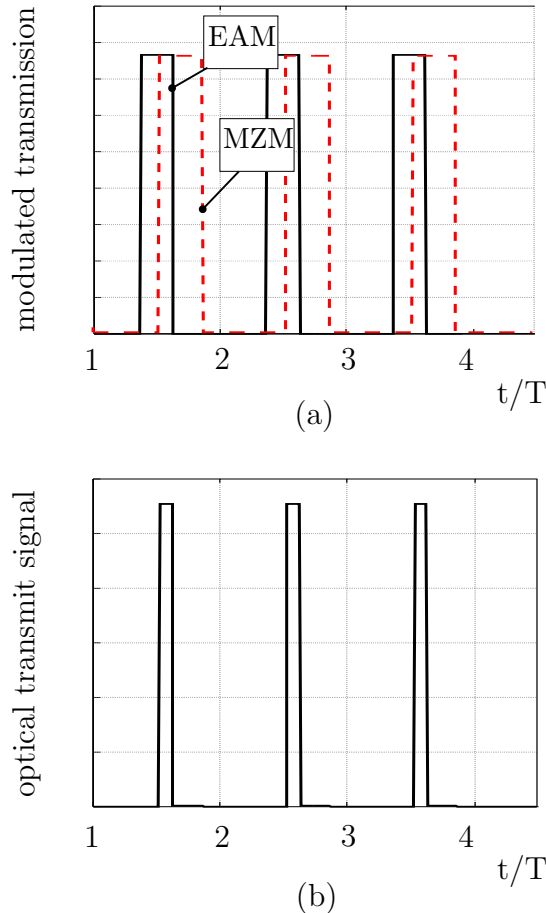


Figure 5.2: Generation of transmit signal. Plot (a) indicates a first optical modulation performed by the an (solid line) and the second made by the MZM (dashed line). Plot (b) shows the resulting optical data signal with high D factor.

A first modulation is performed by an EAM (solid line in Fig. 5.2 (a)). The electrical modulation signal with a duty cycle of 25 % is provided by the pattern generator at the data rate of 1 Gb/s. The data used is a pseudo random bit sequence of length $2^6 - 1$. The optical signal was modulated a second time modulated by an MZM driven with a phase-shifted rectangular signal in order to decrease the duty cycle (see dashed line on Fig. 5.2 (a)). Since the MZM is sensitive to the state of polarization, a polarization controller is placed between the two modulators. The phase shift between the two modulation signals is produced by using cables with proper lengths. The result of the dual-stage modulation is shown in Fig. 5.2 (b). The obtained optical data signal has a D factor of about 9. Figure 5.3 (upper signal) shows the generated optical signal (measured with a digital sampling scope).

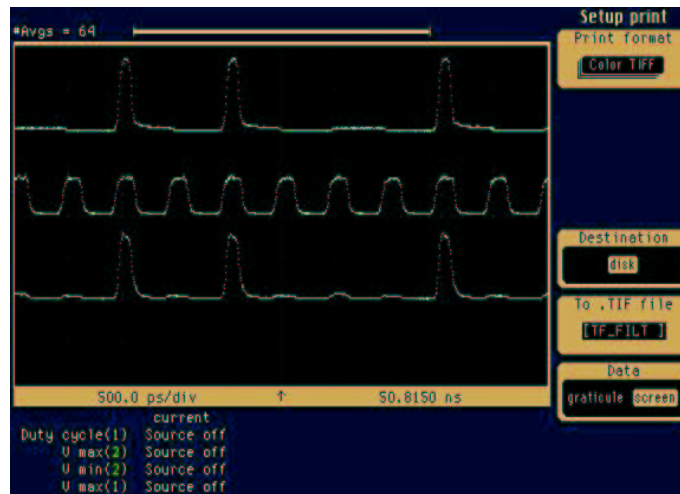


Figure 5.3: Experimental signals: The upper trace is the optical data signal after the MZM; the signal in the center is the time-domain filter function and the lowest trace gives the optically time-domain filtered signal.

The substrate clock signal generated by the pattern generator is also used for generation of the TF function. The signal is split by a 6 dB splitter and input to a high speed XOR-gate. By introducing a phase shift by different cable length an electrical rectangular signal of duty cycle of 22 % is generated. The electrical signal which is the result of the logical operation performed by the XOR gate, is shown as solid line in Fig. 5.4. The signal is used to drive an EAM in the receiver to perform time-domain filtering. Before, a phase shifter (denoted in Fig. 5.1 $\Delta\phi$) allows to manual synchronize the TF function with the data signal. The available range for the synchronization is half a bit. After the phase shifter the signal is electrically amplified and applied to the EAM. Figure 5.3 (center trace) shows the measured TF function used in the experiment. The duty factor of the time-domain filter function amounts to $D_{TF} = 4.5$.

5.1.2 Receiver

The optically preamplified direct-detection receiver employed in the experiment is shown in Fig. 5.1. The receiver consists of

- an erbium doped fiber amplifier (EDFA)
- an optical bandpass filter consisting of a fiber Bragg filter and an optical circulator
- an electroabsorption modulator (EAM)
- a photodiode
- an electrical amplifier
- an electrical lowpass filter (5th order Bessel filter)

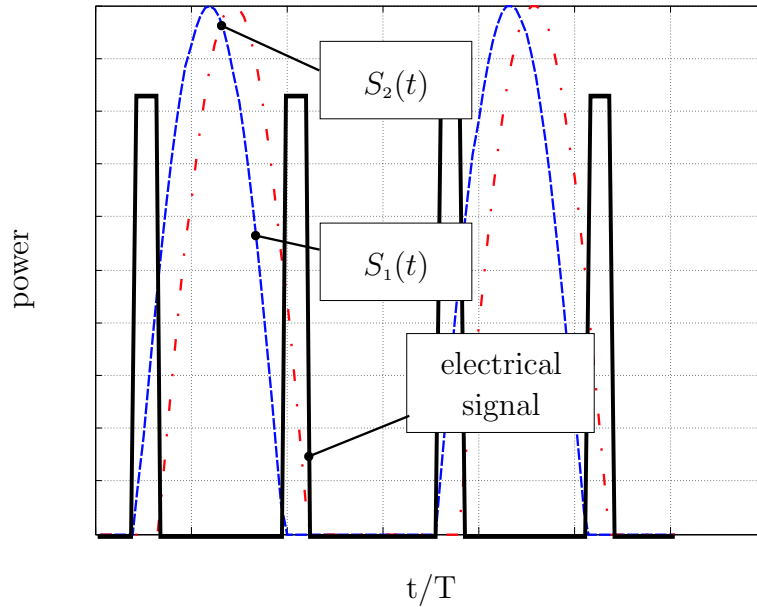


Figure 5.4: Time-domain filter signal generation: The dashed ($S_1(t)$) and dashed-dotted line ($S_2(t)$) are the inputs of the XOR gate (compare Fig. 5.1). The XOR gate (solid line) produces the electrical signal which modulates the EAM to generate the TF function.

- an error counter.

The received signal is preamplified by an EDFA, which provides a gain of about 30 dBm. A fiber Bragg grating in combination with a circulator suppresses ASE noise. The EAM acts a time-domain filtering to further suppress noise (compare center trace in Fig. 5.3). The EAM is followed by a wide bandwidth photodiode which converts the optical power into an electrical current. After electrical amplification and lowpass filtering by an 5th order Bessel filter, an error counter measures the bit error probability of the entire transmission system.

5.1.3 Signal monitoring

A good measurement setup needs several instruments to monitor the signals at different points. The instruments used in our experiment are:

- a wavelength meter
- a digital sampling scope
- a power meter.

Wavelength meter

The center frequency of the optical bandpass filter and the laser emission depend on temperature. While the laser frequency can be manually shifted by varying the internal laser temperature, the central frequency of the optical filter depends on the environmental temperature and could not be controlled. In order to check the alignment of the emitted laser frequency at the optical filter, we use a wavelength meter (denoted by the symbol "λ meter" in Fig. 5.1).

Digital sampling scope

The digital sampling scope allows to visualize the optical and electrical signals. In the following experiments we used it to visualize the transmitted signal and the signal after the time-domain filter.

Optical power meter

The power meter is used to measure the optical input power after the digital attenuator; the latter was used to simulate channel losses.

5.2 Measurements

In this section we present the measurements performed in the optical laboratory in order to experimentally analyze the characteristics of the receiver when a time domain filter is employed. The measured parameter is the *bit error probability (BEP)* of the received signal after the electrical lowpass filter. The *BEP* is plotted logarithmically as a function of the received optical power expressed in dBm, defined as

$$P [dBm] = 10 \log_{10} \left(\frac{P}{1 \text{ mw}} \right). \quad (5.1)$$

5.2.0.1 Basic influence of time-domain filter

The aim of this section is to study the influence of TF on the optical receiver. We consider D factors of the data signal and TF function of 9 and 4.5, respectively. The electrical and the optical filter bandwidth are fixed at $B_e = 1.5 \text{ GHz}$ and $B_o = 1 \text{ nm}$. The value of B_e is chosen to maximize the influence of the TF on the receiver sensitivity. Figure 5.5 shows *BEP* measurements for a system without time-domain filter (dashed line) and with TF (solid line). The gain due to TF is about 0.6, being in good agreement with the simulations results.

5.2.0.2 Measurements at different electrical bandwidths

Figure 5.6 shows the measured influence of the electrical bandwidth on the receiver sensitivity when an optical time-domain filter is employed.

For a large electrical bandwidth of 5 GHz (= 5 R) there is no gain due to TF. When the electrical bandwidth decreases to 2.5 GHz (= 2.5 R), a gain due to temporal filtering

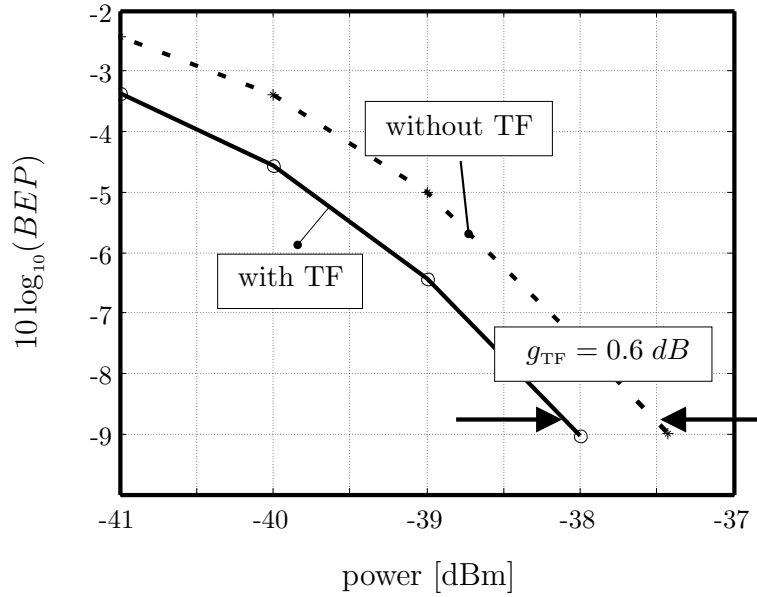


Figure 5.5: Measurement of a system with and without TF. The BEP is expressed as a function of the received power [dBm]. The gain due to TF is about 0.6 dB for the receiver setup chosen. At a data rate of $R = 1$ Gb/s, the electrical and optical filter bandwidths were $B_e = 1.5$ GHz and $B_o = 1$ nm.

of 0.4 dBm was measured. The highest gain of 0.6 dBm was obtained for an electrical bandwidth of 1.5 GHz ($= 1.5 R$). With decreasing the electrical bandwidth the absolute sensitivity decreases [?] since a system using data signals of about 10 % duty cycle asks for a broad electrical bandwidth in order to reach optimum receiver performance. The measurements are in good agreement with the simulation performed in App. 4.

5.2.0.3 Measurements at different optical bandwidth

To study the influence of the optical bandwidth B_o on the receiver sensitivity, we used the following values $B_o = 0.13$ nm, 0.25 nm and 1 nm. The electrical bandwidth was fixed at 1.5 GHz. Figure 5.7 shows the measurement results.

The gain due to time-domain filtering reduces from 0.6 dB for $B_o = 1$ nm to approximated 0.3 dB for the lower two optical bandwidths.

5.3 Comparison of measurements and simulation

In the last section we compare the measurements to the simulations described in App. 4. We will show that there is a good agreement between two different methods used to analyze our optical receiver.

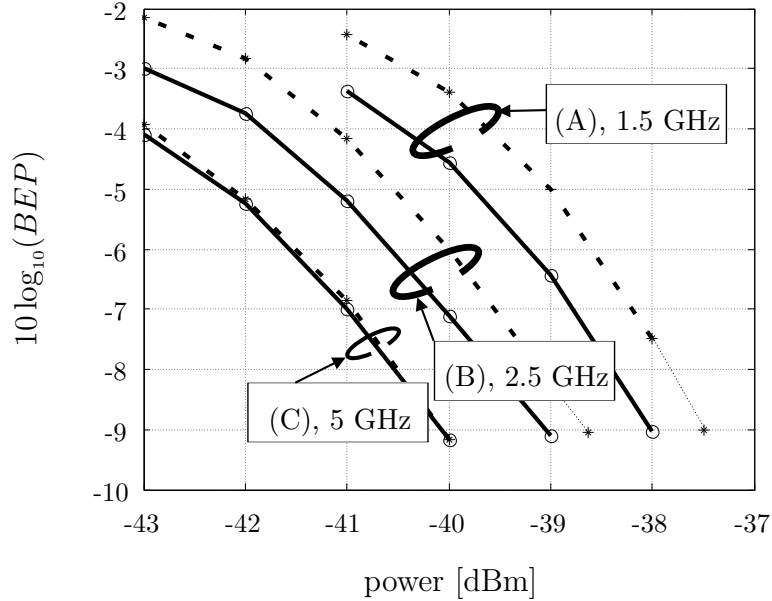


Figure 5.6: Measurement of the influence of electrical filter bandwidth B_e on the gain due to TF. The dashed lines represent the case with TF and the solid lines without. Case (A) is for $B_e = 1.5 \text{ GHz}$; the gain due to TF is $g_{TF} = 0.6 \text{ dB}$. Case (B) applies to $B_e = 2.5 \text{ GHz}$ with $g_{TF} = 0.4 \text{ dB}$. The last case (C) is for $B_e = 1.5 \text{ GHz}$, where g_{TF} is negligible. At a data rate of $R = 1 \text{ Gb/s}$, the optical filter bandwidth was set to $B_o = 1 \text{ nm}$.

5.3.1 Sensitivity dependence on electrical bandwidth

Figures 5.8 (a) and (b) present the results of measurements and simulations when the electrical bandwidth is varied.

Figure 5.8 (a) shows the required receiver power to obtain $BEP = 10^{-9}$ as a function of the electrical filter bandwidth, as obtained in the experiment. The gain due to TF decreases when increasing the electrical bandwidth. When we use an electrical filter with $B_e = 1.5 \text{ GHz}$, the gain due to TF is about 0.6 dB . The gain becomes negligible when the electrical bandwidth is increased to 5 GHz . Simulation results (see Figure 5.8 (b)) give the receiver sensitivity penalty [dB] as a function of B_e . For $B_e = 1.5 \text{ GHz}$, the gain due to TF is about 0.5 dB . With $B_e = 5 \text{ GHz}$ we obtain only a negligible gain due to TF. A clear agreement between measurements and simulations can be seen.

5.3.2 Sensitivity dependence on optical bandwidth

Figures 5.9 (a) and (b) present measurements and simulation results when the optical bandwidth is varied. Figure 5.9 (a) shows the required receiver power [dBm] to reach $BEP = 10^{-9}$ as function of B_o , as obtained in the experiment. Figure 5.9 presents the receiver sensitivity as a function of B_o . The two plots confirm that the gain due to TF is only slightly influenced by B_o and that the gain increases slightly with increasing B_o .

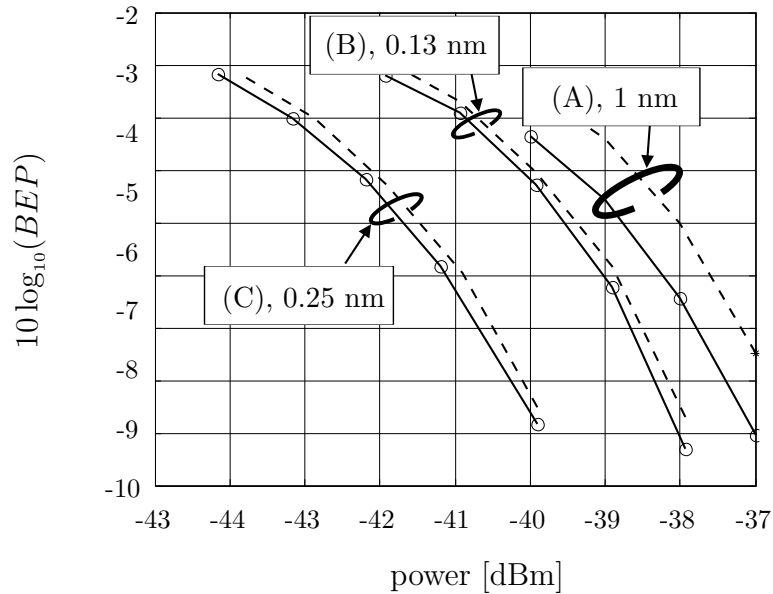


Figure 5.7: Measurement of the influence of optical bandwidth B_o on the gain due to TF. The dashed lines represent the case with TF and the solid line without. In case (A) $B_o = 1 \text{ nm}$, yielding g_{TF} 0.6 dB. Case (B) and (C) are for $B_o = 0.25 \text{ nm}$ and $B_o = 0.13 \text{ nm}$. Here the gain due to TF is only some 0.3 dB. The electrical bandwidth was $B_e = 1.5 \text{ GHz}$, the data rate was $R = 1 \text{ Gb/s}$.

5.3.3 Conclusions

We conclude that measurements and simulations are in reasonable agreement. The gain due to TF and its dependence on electrical and optical bandwidth are confirmed.

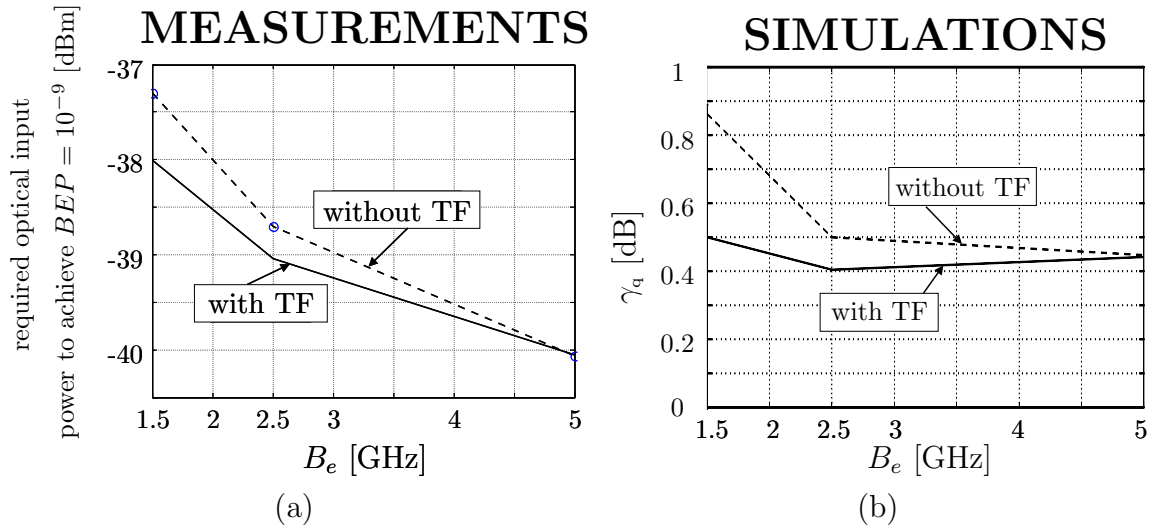


Figure 5.8: Plot (a) shows the experimentally determined received power required for $BEP = 10^{-9}$ as a function of B_e . Plot (b) gives the simulated receiver sensitivity penalty as a function of B_e .

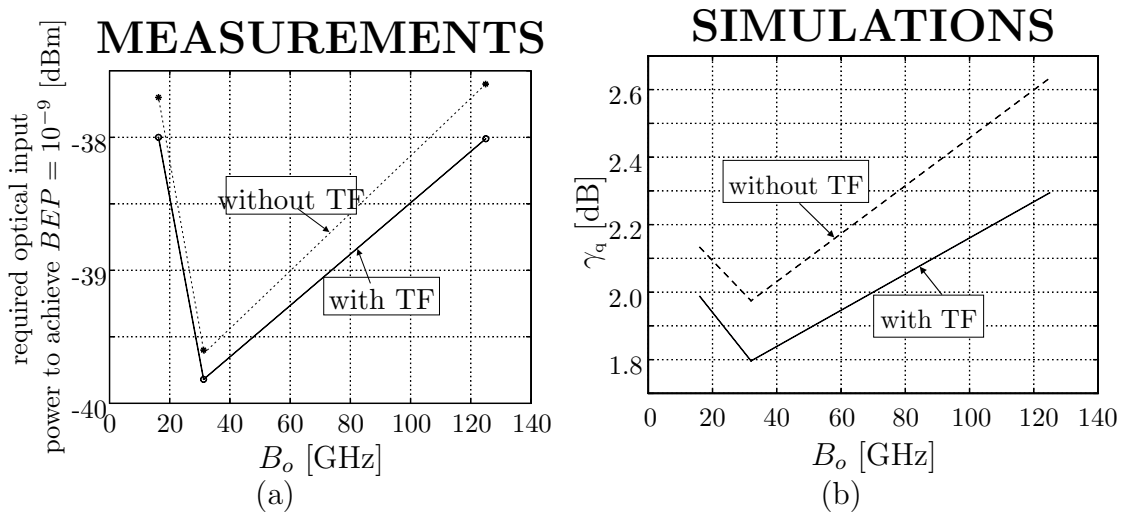


Figure 5.9: Plot (a) shows the experimentally determined received power required for $BEP = 10^{-9}$ as a function of B_o . Plot (b) gives the simulated receiver sensitivity penalty as a function of B_o .

Chapter 6

Summary

This final appendix summarizes of the diploma work presented here. It also presents an application of this work with respect to optical time division multiplexing (OTDM) measurements for high speed systems.

6.1 Summary of the work presented

The aim of the diploma work was to analyze the influence of a time-domain filtering on an optically preamplified direct-detection receiver.

The analysis started giving the theoretical basis (i.e. the noise formulae) of the considered receiver. The noise formulae were obtained by using an advanced Gaussian noise model [?]. Subsequently, the formulae were used to extend `SimTool` for time-domain filtering, including a verification and optimization.

Then we performed simulations in order to determine the influence of TF on the system considered. The first simulations covered the influence of pulse shape and duty cycle of the data signal and the time domain filter function on the receiver sensitivity. We found that a rectangular time-domain filter function in combination with $\cos^2(t)$ -like data signal yields the best results. At the same time we found that the duty factor D must satisfy the condition 4.2 for the case of rectangular pulse and the condition 4.1 for the case of $\cos^2(t)$ -like. Under these conditions the time-domain filter can improve the receiver sensitivity. Further, we investigated the interaction between TF and the electrical and optical bandwidth B_e and B_o . We showed that while B_o has not much influence on the gain g_{TF} in sensitivity obtained by TF, B_e can drastically reduce this gain if it is much larger than the data rate R . We found that the TF only reduces the ASE-ASE beat noise. This explains the small gain due to TF, since the most important noise source namely signal-ASE beat noise is not suppressed by the TF. Finally, we considered the parameters extinction ratio (ζ_{TF}) and the misalignment (Δt_{TF}) of the time-domain filter. For the first parameter we found that a value of 12 dB is sufficient to reach maximum g_{TF} . For the second parameter we found an upper limit. When Δt_{TF} is smaller than the upper limit, there is no degradation due to TF.

In the next step experiments were performed at the optical laboratory. By measuring

the bit error probability (*BEP*), determined the sensitivity of an optical receiver with and without TF. We performed measurements covering the influence of B_e and B_o on the time-domain filtering gain. These measurements confirmed the simulations. In particular, it was shown that B_o does not influence strongly g_{TF} , in contrast B_e has a strong influence on g_{TF} .

Theory and experiments proved that a time-domain filter can only slightly improve the receiver sensitivity of an optically preamplified DD receiver. The improvement can only be obtained when the value of the two D factors are high (e.g. $D_{\text{TF}} > 5$, $D > 5$), when the value of B_e is smaller than $2R$, and if $\zeta_{\text{TF}} \geq 12$ dB.

6.2 Application: OTDM measurements

This last section presents as application of the diploma thesis a work about OTDM measurements for high speed systems. These research results are going to be published under the title "Emulating ETDM receivers by OTDM receivers for high speed system measurements". The mention article was written in collaboration with M.M.Strasser and P.J.Winzer and was accepted for publication at the conference LEOS Annual Meeting 2002, Glasgow (UK).

Today, the optical time domain multiplexing (OTDM) measurements for high speed systems are an important topic in the optical communications researches. In the last years, commercial optical systems at the data rate of 40 Gb/s were developed. The push for higher data rate has always left behind the development of high-speed detection electronics. This produced a gap between the speed of the transmission and the detection in high speed systems. To solve this problem research laboratories developed an alternative technique to measure the performance of such a systems. The idea was to emulate an electrical time domain multiplexing (ETDM) receiver by an OTDM receiver. For instance, in a 40 Gb/s system, the information is divided in 4 channels with 10 Gb/s, each channel can be separately detected receiver with slower electronics [27]. Later fast ETDM receivers became commercially available [28] and today still, the question is how closely OTDM receivers resemble ETDM receivers, both in terms of absolute sensitivity and robustness to performance degrading effects.

The aim of the article is to point out similarities and differences between the two receivers concepts, both by means of theory and experiment. To have a good control over the experimental parameters, we performed the measurements at 10 Gb/s (ETDM) and $4 * 2.5$ Gb/s (OTDM). Figure 6.1 shows the experimental setup. The common input signal was at 10 Gb/s with a duty cycle of 45 %. The upper eye diagrams in Fig. 6.1 correspond to the signal present in ETDM receiver, for which the electroabsorption modulator (EAM) was not modulated, letting the spectrally filtered data pulses directly reach the photodiode. The lower eye diagrams represent the waveforms found in an OTDM receiver, which was realized by driving the EAM with rectangular electrical signal with a duty cycle of 25 %. In this way, four tributaries, at a reduced rate of 2.5 Gbit/s, were generated by time-domain filtering. The extinction ratio ζ_{TF} of the EAM

was 18 dB. The opto-electronic conversion was performed, for both receivers alike, by a wideband (40 GHz) photodiode. The detection was followed by 5th-order Bessel filter. For the ETDM receiver, we chose $B_e = 7 \text{ GHz}$, for the OTDM receiver we chose a filter bandwidth of $B_e = 1.5$

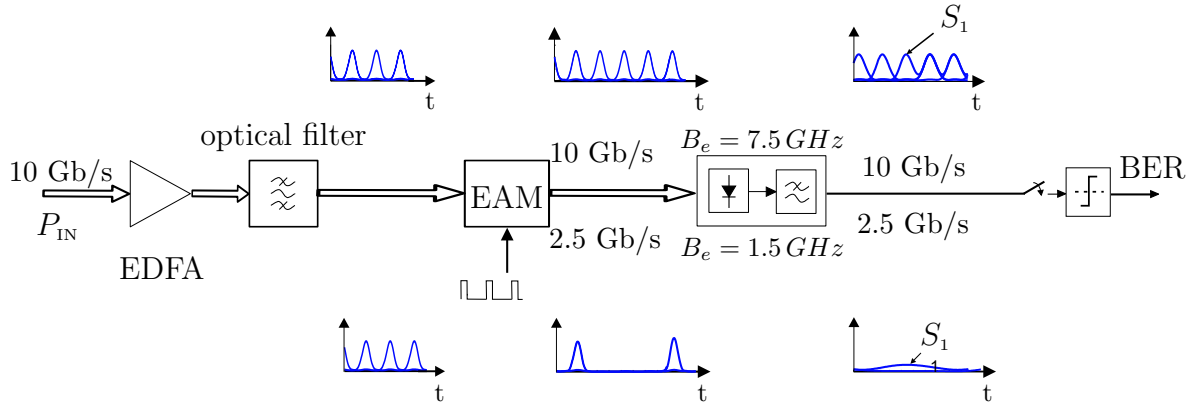


Figure 6.1: Experimental setup of ETDM receiver (upper signals) and OTDM receiver (lower signals). The EAM (i.e. the optical demultiplexer) converts the ETDM receiver to an OTDM receiver.

Figure 6.2 shows the BEP measurement results for an optical bandwidth of $B_o = 25 \text{ GHz}$. Equal performance of all the four tributaries of the OTDM receiver was confirmed. The sensitivity difference between the OTDM and the ETDM receiver amounts to about 1 dBm. It was shown in Sect. 4.1 and 5.2.0.1 that the time-domain filter function may improve the sensitivity at the optical receiver by about 0.6 dBm. In the present setup a similar improvement is measured.

We conclude that the experiments and simulations show an useful application of the studies about time-domain filtering. The analysis can explain in part why an OTDM receiver has a better absolute sensitivity than an ETDM receiver. The absolute difference in terms of receiver sensitivity is about 1 dBm. A difference of about 0.6 dBm is directly related to the gain due to the time-domain filtering.

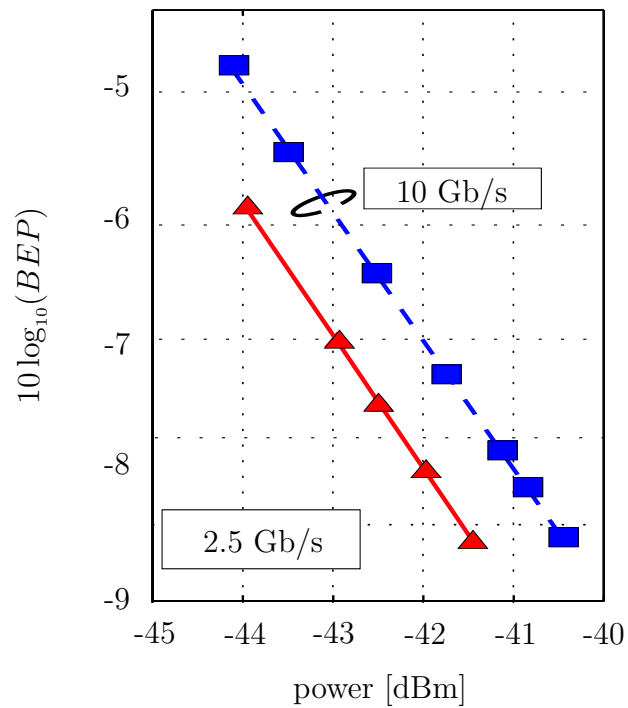


Figure 6.2: Measurement of the BEP of an ETDM receiver (dashed line) and an OTDM receiver (solid line). It was confirmed that the four tributaries of the OTDM system have the same BEP. The difference between the BEP of the two systems, expressed in terms of receiver sensitivity, is about 1 dBm.

Bibliography

Bibliography

- [1] M. M. Strasser, M. Pfennigbauer, M. Pauer, and P. J. Winzer, “Experimental verification of optimum filter bandwidths in direct-detection (N)RZ receivers limited by optical noise,” *Proc. 14th Annual Meeting of LEOS*, vol. 2, pp. 485–486, 2001.
- [2] P. J. Winzer, M. Pfennigbauer, M. M. Strasser, and W. Leeb, “Optimum filter bandwidth for optically preamplified (N)RZ receivers,” *J. Lightwave Technol.*, vol. 19, pp. 1263–1273, 2001.
- [3] E. Desurvire, “Erbium-doped fiber amplifiers,” *John Wiley & Sons*, 1994.
- [4] W. Leeb, “Optische Nachrichtentechnik,” *lecture notes, Vienna University of technology*, 1996.
- [5] P. J. Winzer, A. Kalmar, and W. Leeb, “Intersatellite laser communication at $1.5\ \mu\text{m}$: chances and problems,” ESA contract report, Contract No. 11846/96/NL/SB(SC), Insitiut für Nachrichtentechnik und Hochfrequenztechnik, Technische Universität Wien, 1998.
- [6] G. Einarsson, *Principles of lightwave communications*. John Wiley & Sons, Inc., 1996.
- [7] P. J. Winzer, “Receiver noise modeling in the presence of optical amplification,” *Proc. Optical Amplifiers and Their Applications (OAA'01), July 1-4, Stresa (Italy), paper OTuE16*, 2001.
- [8] P. J. Winzer, “Optically preamplified receiver with low quantum limit,” *Electronics letters*, vol. 37, p. 582, 2001.
- [9] P. Becker, N. Olsson, and J. Simpson, *Erbium-doped fiber amplifiers. Fundamentals and technology*. Academic Press, New York, 1999.
- [10] P. J. Winzer and A. Kalmar, “Sensitivity enhancement of optical receivers by impulsive coding,” *J Lightwave Technol.*, vol. 17, pp. 171–177, 1999.
- [11] M. Pfennigbauer, P. J. Winzer, M. M. Strasser, and W. Leeb, “Optimum optical and electrical filter characteristics in optically preamplified direct detection (N)RZ receivers,” *Proc. of SPIE, Free-Space Laser Communication Technologies XIII*, vol. 4272, pp. 160–169, 2001.

- [12] M. M. Strasser, P. Winzer, and A. Napoli, "Emulating of ETDM receivers by OTDM receiver for high speed system measurement," *accepted for publication to LEOS'2002, Annual Meeting, Glasgow (UK)*, 2002.
- [13] L. Mandel and E. Wolf, *Optical coherence and quantum optics*. Cambridge University Press, 1995.
- [14] H. Weinrichter and F. Hlawatsch, *Stochastische Grundlagen Nachrichtentechnischer Signale*. Springer-Verlag Wien New York, 1991.
- [15] M. M. Strasser, "Optical free-space transmitters and their effects on preamplified direct detection," *Ph.D. thesis, Technische Universität Wien (Austria)*, 2001.
- [16] S. Danielsen, B. Mikkelsen, T. Durhuus, and *et. al*, "Detailed noise statistics for an optically preamplified direct detection receiver," *J. Lightwave Technol.*, vol. 13, pp. 977–981, 1995.
- [17] J. Lee and C. Shim, "Bit-error-rate analysis of optically preamplified receivers using an eigenfunction expansion method in optical frequency domain," *J. Lightwave Technol.*, vol. 12, pp. 1224–1229, 1994.
- [18] G. Jacobsen, *Noise in digital optical transmission systems*. Artech House, 1994.
- [19] B. Saleh and M. Teich, *Fundamentals of photonics*. New York: Wiley, 1991.
- [20] G. Reider, *Photonik / Eine Einführung in die Grundlagen*. Springer-Verlag Wien New York, 1997.
- [21] A. Ohtonos and K. Kalli, *Fiber Bragg Gratings*. Artech House, 1999.
- [22] T. Wood, "Multiple quantum well (MQW) waveguide modulators," *J. Lightwave Technol.*, vol. 6, pp. 743–757, 1988.
- [23] S. Oshiba, K. Nakamura, and H. Horikawa, "Low-drive-voltage MQW electroabsorption modulator for optical short-pulse generation," *J. Quantum Electron.*, vol. 34, pp. 277–281, 1998.
- [24] K. Yoshino, T. Takeshita, I. Kotaka, and *et. al*, "Compact and stable electroabsorption optical modulator modules," *J. Lightwave Technol.*, vol. 17, pp. 1700–1707, 1999.
- [25] M. Suzuki, H. Tanaka, N. Edagawa, and *et. al*, "Transform-limited optical pulse generation up to 20-GHz repetition rate by a sinusoidally driven InGaAsP electroabsorption modulator," *J. Lightwave Technol.*, vol. 11, pp. 468–473, 1993.
- [26] D. Johnson, J. Johnson, and H. Moore, *A handbook of active filters*. Englewood Cliffs, NJ: Prentice-Hall, 1980.
- [27] D. Garthe *OFC'97*, vol. PD20, 2002.
- [28] T. N. Nielsen *ECOC'99*, vol. PD2-2, 2002.